

Diffusion Processes on Small-World Networks with Distance-Dependent Random-Links

Balázs Kozma*

*Laboratoire de Physique Théorique (UMR du CNRS 8627),
Bâtiment 210 Université Paris-Sud - 91405 Orsay Cedex, France*

Matthew B. Hastings†

*Center for Non-linear Studies and Theoretical Division,
Los Alamos National Laboratory, Los Alamos, New Mexico 87545, USA*

G. Korniss‡

*Department of Physics, Applied Physics, and Astronomy,
Rensselaer Polytechnic Institute, 110 8th Street, Troy, NY 12180-3590, USA*

We considered diffusion-driven processes on small-world networks with distance-dependent random links. The study of diffusion on such networks is motivated by transport on randomly folded polymer chains, synchronization problems in task-completion networks, and gradient driven transport on networks. Changing the parameters of the distance-dependence, we found a rich phase diagram, with different transient and recurrent phases in the context of random walks on networks (or with different smooth and rough phases in the context of noisy task-completion landscapes). We performed the calculations in two limiting cases: in the case of rapid-network-update, where the rearrangement of the random links is fast, and in the quenched case, where the link rearrangement is slow compared to the motion of the random walker or the surface. It has been well-established that in a large class of interacting systems, adding an arbitrarily small density of, possibly long-range, quenched random links to a regular lattice interaction topology, will give rise to mean-field like behavior (i.e., the small-world-like random links can be treated in a mean-field fashion). In some cases, however, mean-field scaling breaks down in "low-dimensional" small-world networks, where random links are added to a low-dimensional regular structure. Examples of such cases are the common diffusion and the Edwards-Wilkinson process, the main subjects of this paper. This break-down can be understood by treating the random links perturbatively, where the mean-field prediction appears as the lowest-order term of a naive perturbation expansion. The asymptotic analytic results are also confirmed numerically by employing exact numerical diagonalization of the network Laplacian. Further, we construct a finite-size scaling framework for the relevant observables, capturing the cross-over behaviors in finite networks. This work provides a detailed account of the self-consistent-perturbative and renormalization approaches briefly introduced in Refs. [1] and [2].

PACS numbers: 89.75.Hc, 05.40.Fb, 05.60.Cd 68.35.Ct,

I. INTRODUCTION

Our environment is pervaded by large-scale complex systems, rooted in different backgrounds: sociology, decision-making, economy, transportation, ecology, regulation and transport in biology, information transfer, and so on [3, 4, 5]. The major characteristic of these systems is that they do not have any regular structure, and they exist over complex networks. Characterizing these networks is a nontrivial task, and finding the most important quantities to classify the static structure of them has been intensely researched. Recent research on networks has shifted the focus from the structural (topological) analysis to the study of processes (dynamics) on

these complex networks [6].

One of the most common phenomena that occur in a large number of processes is diffusion, where the flow across the links, and consequently, the rate of change of a generalized density at a given node, is driven by the local density gradients between the nodes and its neighbors. Therefore, it is important to understand the properties of the diffusion and the related diffusion-operator (or Laplace-operator) on these networks. In our work, besides the results, we present a technique, based on impurity-averaged perturbation theory, which gives a novel tool to study processes on networks especially *small-world* networks.

First introduced by Watts and Strogatz [7, 8], small-world networks were constructed to model social interactions [9]. In the original construction, on a regular lattice, each node is connected to k nearest neighbors, then each link of a node is rewired to a randomly chosen node with probability p . Changing the value of p , one can interpolate between a regular ($p = 0$) and a completely ran-

*Electronic address: kozmab@th.u-psud.fr

†Electronic address: hastings@lanl.gov

‡Electronic address: korniss@rpi.edu

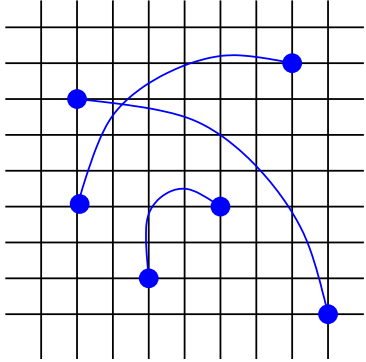


FIG. 1: Schematic construction of a small-world network

dom, Erdős-Rényi, network ($p = 1$) [10, 11]. The original construction of Watts and Strogatz was difficult to treat mathematically so a new construction was suggested [12] combining two networks: a regular d -dimensional one, and on the top of that an Erdős-Rényi network (see Fig. 1) with parameter p . We refer to this construction as the “plain” SW network in order to distinguish it from power-law SW networks, defined later. Well known classical models (originally defined on regular lattices) have been studied on these networks, such as the Ising model [13, 14, 15, 16, 17], the XY model [18], diffusion [19, 20, 21, 22, 23, 24, 25, 26, 27], and synchronization [28, 29, 30, 31, 32, 33].

In this paper, we consider a class of networks, called *power-law small-world* (PL-SW) networks [21, 34, 35, 36]. In these networks, on top of a regular d -dimensional lattice, the random long-range links have a *distance-dependent power-law probability distribution*, where the probability of two nodes being connected is give by

$$\text{Probability } (i \text{ and } j \text{ connected}) = \frac{p}{\mathcal{N}r^\alpha} = pf(r). \quad (1)$$

Here, $r = |i-j|$ is the Euclidean distance between the two nodes in the original regular lattice, α is the strength of the distance-dependent suppression of the random long-range links, and p is the density of such long-range links (i.e., p is the average number of random links on a node.) \mathcal{N} is the normalization-factor of the distribution

$$\mathcal{N} = \sum_{i=1}^{L^d} \frac{1}{r^\alpha}, \quad (2)$$

where L is the linear size of the d -dimensional lattice.

Both the structure of these networks [37] and diffusive dynamics on these networks [21] have been studied by others, in one dimension. Our results provides a detailed exploration of the phase diagram in diffusion processes as the connection topology interpolates between the original “plain” SW ($\alpha = 0$) and the purely short-range connected ($\alpha = \infty$) network. One expects that when the probability of the random links decays rapidly enough ($\alpha \rightarrow \infty$), the large scale behavior of the processes on

them is not affected by these links. When the probability of the random links decays slowly ($\alpha \rightarrow 0$), the results of the original SW network should be recovered [1, 38]. In between, there is a transition which is the focus of this paper. Our starting point is a calculation on rapidly-updated networks which turns out to be the first-order approximation of a naive perturbation expansion for the quenched system. For small p , this expansion breaks down and we apply a self-consistent calculation.

Earlier numerical work [21] for $d = 1$, in the context of the random-walk, suggested that a crossover from the transient to the recurrent phase occurs at around $\alpha \approx 2$. Here, we compute the asymptotic scaling properties of the propagator analytically (and confirm it numerically in $d = 1$), and precisely construct the full phase diagram for all d . This work provides a detailed account of the self-consistent perturbative approach, briefly introduced in Refs. [1] and [2], and expanded numerical results.

In our research we will consider different diffusion-driven processes, defined in the following sections, on these networks. Two different cases will be distinguished: the *rapidly-updated* network, when the rearrangement of the random links on the network takes place on a timescale much faster than the process itself, and the *quenched* network, when the random links can be considered static with respect to the timescale of the process. In the network literature, the first case of rapidly-updated networks is often referred to as *annealed* networks, and we will refer to them as annealed in this manuscript also. We will denote the annealed average of a quantity by $[\dots]^{ann}$ and the quenched average by $[\dots]$. In many cases, in the quenched system, the effect of the random long-range links can be understood by a general criterion [38], based on averaging over the long-range links in a mean-field (or annealed) fashion (see Section II.). For a few models, this criterion is violated, leading to non-mean-field behavior such as diffusion on a small-world network with a one-dimensional spatial structure.

Such a power-law SW network can emerge in a randomly-folded polymer where, besides the one-dimensional chain of the monomers, two distant monomers can be adjacent to each other, facilitating random long-range links, because of the spatial conformation of the polymer [39]. For example, in three dimensions, for an ideal chain, the probability of two distant sites to be adjacent is proportional to $r^{-3/2}$ where r is the distance of the two segments, while for a polymer chain in a good solvent, this probability is proportional to $r^{-1.97}$ [40]. Note, that in the case of small-world networks generated by such polymer configurations, the random links are correlated: there is a high chance to find an other long-range link around an existing one of the same length scale. In the case of annealed networks, these correlations are “washed away” by the constant rearrangements of the links but, in the quenched case, the correlations can change the universal, large scale, behavior of the processes on them. In our study, we will deal with uncorrelated random links and leave the correlated case for

further research.

Another field where such structure can emerge is that of synchronization problems in distributed computing [33, 41] where synchronization is achieved by introducing random communications between distant processors. Choosing a power-law SW network may be preferable as it lowers the cost associated with communications. It was also argued that “wiring-cost” considerations [42] for spatially embedded networks, such as cortical networks [43] or on-chip logic networks [44], can generate such power-law suppressed link-length distribution. In general, wiring cost in SW networks can result to the introduction of power-law SW networks [42].

A. Diffusion processes

One case in which the diffusion equation arises on a PL-SW network is a macromolecule randomly moving along a polymer chain jumping over adjacent segments with nonzero probability [21, 35, 45, 46]; if the macromolecule motion is fast compared to rearrangements of the links, then the network may be considered as quenched, while if the macromolecule motion is slow compared to the link rearrangements then the network is annealed [47]. The equation describing random walk processes is

$$\partial_t P_{\mathbf{r}'}(t) = - \sum_{\mathbf{r}''} (\Delta_{\mathbf{r}',\mathbf{r}''}^0 + q\Delta_{\mathbf{r}',\mathbf{r}''}^{rnd}) P_{\mathbf{r}''}(t), \quad (3)$$

where $P_{\mathbf{r}'}(t)$ is the probability of finding the walker at site \mathbf{r}' at time t and q is the relative *transition rate* through the random links. Above we have used that the diffusion operator $\Delta_{\mathbf{r},\mathbf{r}'}$ on SW networks, embedded in regular d -dimensional networks, can be written as

$$\Delta_{\mathbf{r},\mathbf{r}'} = \Delta_{\mathbf{r},\mathbf{r}'}^0 + q\Delta_{\mathbf{r},\mathbf{r}'}^{rnd}, \quad (4)$$

where Δ^0 is the regular d -dimensional Laplace operator on the underlying lattice, $\Delta_{\mathbf{r},\mathbf{r}'}$ is the Laplacian on the random part of the network, and q is the relative strength of the relaxation through the random links. For example, in one dimension, $\Delta_{ij}^0 = 2\delta_{i,j} - \delta_{i,j-1} - \delta_{i,j+1}$. The diffusion through the random links is

$$\Delta_{\mathbf{r},\mathbf{r}'}^{rnd} = \begin{cases} -A_{\mathbf{r},\mathbf{r}'}^{rnd} & \text{if } \mathbf{r} \neq \mathbf{r}', \\ \sum_{\mathbf{r}'' \neq \mathbf{r}} A_{\mathbf{r},\mathbf{r}''}^{rnd} & \text{if } \mathbf{r} = \mathbf{r}' \end{cases} \quad (5)$$

where $A_{\mathbf{r},\mathbf{r}'}^{rnd} = 1$ if there is a random long-range link connecting sites \mathbf{r} and \mathbf{r}' . For PL-SW networks [see Eq. (1)],

$$\text{Probability } (A_{\mathbf{r},\mathbf{r}'}^{rnd} = 1) = \frac{p}{\mathcal{N}|\mathbf{r} - \mathbf{r}'|^\alpha} = pf(|\mathbf{r} - \mathbf{r}'|)$$

$$\text{Probability } (A_{\mathbf{r},\mathbf{r}'}^{rnd} = 0) = 1 - pf(|\mathbf{r} - \mathbf{r}'|). \quad (6)$$

For technical purposes, it is often useful to employ the *spectral decomposition* of the diffusion operator. In the orthogonal eigensystem:

$$\Delta\Psi^k = \lambda_k\Psi^k \quad (7)$$

for all k -s, where Ψ^k is the normalized eigenvector and λ_k is the corresponding eigenvalue of the operator and

$$\langle\Psi^k|\Psi^l\rangle = \delta_{kl}. \quad (8)$$

The $i = 0$ index is reserved for the uniform zero-mode of the system:

$$\lambda_0 = 0 \quad (9)$$

and

$$\Psi^0 = \frac{1}{\sqrt{L^d}}(1, 1, 1, \dots, 1). \quad (10)$$

The Green's function, $G_{\mathbf{r}',\mathbf{r}''}(t)$, of the diffusion process is the solution of the diffusion equation with initial condition $P_{\mathbf{r}'}(t = 0) = \delta_{\mathbf{r}',\mathbf{r}''}$. Because the diffusion equation has only a first-order time derivative, formally its solution can be written as

$$\begin{aligned} G_{\mathbf{r},\mathbf{r}''}(t) &= \sum_{\mathbf{r}'} \left(e^{-(\Delta^0 + q\Delta^{rnd})t} \right)_{\mathbf{r},\mathbf{r}'} P_{\mathbf{r}'}(t = 0) \\ &= \left(e^{-(\Delta^0 + q\Delta^{rnd})t} \right)_{\mathbf{r},\mathbf{r}''}. \end{aligned} \quad (11)$$

Using the spectral decomposition of the diffusion operator one obtains

$$e^{-(\Delta^0 + q\Delta^{rnd})t} = \sum_k e^{-\lambda_k t} |\Psi^k\rangle\langle\Psi^k|, \quad (12)$$

where $(|\Psi^k\rangle\langle\Psi^k|)_{\mathbf{r},\mathbf{r}'} = \Psi_{\mathbf{r}}^k\Psi_{\mathbf{r}'}^k$ is the projector to the subspace of Ψ^k . It is often useful to introduce the Laplace transform of the Green's function, $G_{\mathbf{r}',\mathbf{r}''}(\omega) = \int_0^\infty G_{\mathbf{r}',\mathbf{r}''}(t)e^{-\omega t}dt$. Performing the integration over the time domain, one finds

$$G_{\mathbf{r}',\mathbf{r}''}(\omega) = (\Delta^0 + q\Delta^{rnd} + \omega)_{\mathbf{r}',\mathbf{r}''}^{-1}. \quad (13)$$

In order to characterize the diffusion process on different networks, one of our focuses is on the scaling properties of the *expected number of returns* of the random walker by time T . For one node at site \mathbf{r} , it is defined as

$$\begin{aligned} F_{\mathbf{r}}(T) &= \int_0^T dt P_{\mathbf{r}}(t) \\ &= \int_0^T dt G_{\mathbf{r},\mathbf{r}}(t). \end{aligned} \quad (14)$$

Averaging over all nodes in the network one then has

$$F(T) = \frac{1}{L^d} \sum_{\mathbf{r}} \int_0^T dt G_{\mathbf{r},\mathbf{r}}(t). \quad (15)$$

We are interested in its long-time behavior in the thermodynamic limit. A random-walk process is called *recurrent* if in an infinite system, the expected number of returns is infinite as $T \rightarrow \infty$ and *transient* if, on average, the

walker visits the origin only finite number of times. Using the spectral decomposition of $G_{\mathbf{r},\mathbf{r}}(t)$ from Eq. (12), one obtains

$$\begin{aligned} F(T) &= \frac{1}{L^d} \int_0^T \sum_k e^{-\lambda_k t} \sum_{\mathbf{r}} |\Psi_{\mathbf{r}}^k|^2 dt \\ &= \frac{1}{L^d} \sum_k \int_0^T e^{-\lambda_k t} dt \\ &= \frac{1}{L^d} \sum_{k \neq 0} \frac{1}{\lambda_k} (1 - e^{-\lambda_k T}) + \frac{T}{L^d}. \end{aligned} \quad (16)$$

The above form is useful for exact numerical calculations for a given realization of the network.

To analytically extract the leading-order asymptotic scaling properties for $F(T)$, instead of the sharp cutoff, it is sufficient to use a kernel that suppresses the integrand for $t \gg T$. To make our calculation easier, we chose $\int_0^\infty G_{\mathbf{r},\mathbf{r}}(t) e^{-t/T} dt$ [48]. From the spectral decomposition of the Green's function, and repeating the same steps as above, now for the exponential cutoff, one finds

$$F(T) \propto \frac{1}{L^d} \sum_{\mathbf{r}} G_{\mathbf{r},\mathbf{r}}(\omega = 1/T) = \frac{1}{L^d} \sum_{k \neq 0} \frac{1}{\lambda_k + 1/T} + \frac{T}{L^d}. \quad (17)$$

In order to make the formalism similar to that of the other phenomena described in this section, let us introduce a modified GF,

$$\hat{G}_{\mathbf{r},\mathbf{r}'}(\omega) = G_{\mathbf{r},\mathbf{r}'}(\omega) - \frac{1}{\omega L^d}. \quad (18)$$

It is basically the GF defined in the space orthogonal to the uniform zero mode. Note that, in the next section, defining the GF in this subspace will be necessary because the coupling matrix is non-invertible. In terms of this modified GF

$$F(T) \propto \frac{1}{L^d} \sum_{\mathbf{r}} \hat{G}_{\mathbf{r},\mathbf{r}}(\omega = 1/T) + \frac{T}{L^d}. \quad (19)$$

B. Synchronization in task-completion networks and the Edwards-Wilkinson process

In this section, we motivate the Edwards-Wilkinson (EW) process [49] on networks, which can be thought of in terms of a synchronization paradigm in a noisy environment. Consider a distributed task-processing network, where the processing nodes, in order to schedule and perform new tasks, must *wait* for the results delivered by other nodes. This task-dependency between nodes correspond to the links, which in general, can be asymmetric or directed, quenched or time-dependent. Examples include distributed-computing systems [41], manufacturing supply chains, or e-commerce-based services facilitated by interconnected servers [50]. Understanding the scaling behavior of the fluctuations in our model

will help us better understand the generic features of delays and back-log formation in large-scale networked processing systems. In particular, for certain distributed computing schemes (parallel discrete-event simulations) [51, 52, 53, 54, 55, 56], it was shown [57] that on regular grids, the evolution of the task-completion (or synchronization) landscape is governed by the Kardar-Parisi-Zhang (KPZ) [58] equation. The resulting landscape is “rough”, corresponding to a large spread in the locally-completed tasks on different nodes. In general, the width provides a sensitive measure of the average degree of desynchronization in task-completion networks,

$$w^2(t) = \frac{1}{N} \sum_{i=1}^N (h_i(t) - \bar{h}(t))^2. \quad (20)$$

Here, $h_i(t)$ is the local progress on node i , $\bar{h} = (1/N) \sum_{i=1}^N h_i(t)$ is the mean progress, and N is the number of processing nodes in the system. When the network has an underlying d -dimensional structure with linear size L , one also has $N = L^d$.

In order to improve the uniformity of the progress of the nodes in the above distributed-computing example, ultimately leading to better scalable performance, one must suppress large fluctuation in the synchronization landscape. For example, one can construct a scalable autonomous synchronization schemes where the nodes, in addition to their nearest neighbor on the grid, also communicate with random (possibly distant) neighbors (with a very low frequency); the sole purpose of communications through the random links is to keep the spread of the task-completion landscape under control [33, 41]. In this case, the underlying synchronization network is a SW network (which can be quenched or annealed, depending on the implementation).

While the precise local synchronization rules give rise to strongly non-linear effective interactions between the nodes, one can gain some insight by considering the linearized version of the effective equations of motion. As it was shown for the basic distributed-computing synchronization problem [57], the dynamics, neglecting nonlinearities, can be effectively captured by the EW process [49]. The generalization of the EW process to complex networks [1, 2] (focusing on PL-SW networks in this paper), is given by

$$\partial_t h_i(t) = - \sum_j \Delta_{ij} h_j(t) + \eta_i(t), \quad (21)$$

where Δ_{ij} is the diffusion operator *on the network* and $\eta_i(t)$ (without loss of generality) is a delta-correlated white noise with variance 2 :

$$\langle \eta_i(t) \eta_j(t') \rangle = 2 \delta_{ij} \delta(t - t'). \quad (22)$$

In general, the symmetric relaxational couplings between the nodes, A_{ij} ($A_{ii} \equiv 0$), can be weighted. The generalized network Laplacian then can be written as

$$\Delta_{ij} = \delta_{ij} \sum_k A_{ik} - A_{ij}. \quad (23)$$

For unweighted networks with unit coupling strength A_{ij} is simply the adjacency matrix.

Clearly, the precise scaling behavior of synchronization landscape (its width, in particular) is strongly affected by *both* the nonlinearities and the underlying interaction topology. Our results provide a detailed account on the network's effect on the EW synchronization problem. Because of the linear nature of the model, this is a much simpler problem than the actual synchronization dynamics, but, as we shall see in the following sections, the behavior of it is still nontrivial, particularly on quenched SW networks. The understanding of the EW process (on networks) is a necessary first step before tackling more complicated, nonlinear problems.

Using the Fokker-Planck description of the EW process, it can be shown [59] that the steady-state probability distribution function (PDF) of the possible surface configurations is

$$P[\vec{h}] \propto \exp\left(-H[\vec{h}]\right), \quad (24)$$

where $\vec{h} = \{h_i\}_{i=1}^{L^d}$ is the configuration-vector and $H[\vec{h}]$ is the steady-state Hamiltonian[81] of the surface

$$H[\vec{h}] = \frac{1}{2} \sum_{ij} h_i \Delta_{ij} h_j = \frac{1}{2} \sum_{ij} A_{ij} (h_i - h_j)^2. \quad (25)$$

The steady-state Green's function (GF) or *propagator* of the system is defined as the two-point correlation function. Since the steady-state PDF is Gaussian, the two-point correlation function is the inverse of the coupling matrix. In our case, Δ is non-invertible because of the uniform eigenmode Ψ^0 with zero eigenvalue [Eq. (10)]. The singularity of this mode can also be traced back to Eq. (21), in that the mean height performs a simple random walk and has a diverging variance in the limit of $t \rightarrow \infty$ (for any system size), i.e., its steady-state variance does not exist. Equivalently, the steady-state PDF Eq. (24) with the Hamiltonian Eq. (25) is ill-defined, $\langle \bar{h}^2 \rangle = \infty$. This problem can be overcome by constructing observables which lie in the space orthogonal to the zero mode of the network Laplacian. It can be achieved by, e.g., measuring height fluctuations from the mean [see Eq. (20)]. Hence, the appropriately defined GF is

$$G_{ij} = \langle (h_i - \bar{h})(h_j - \bar{h}) \rangle = \hat{\Delta}_{ij}^{-1} \quad (26)$$

where $\hat{\Delta}^{-1}$ is the inverse of Δ in the space orthogonal to the uniform zero mode. Particularly useful for numerical purposes, one can employ the spectral decomposition of the inverse of the network Laplacian in the space orthogonal to the zero mode [82]

$$G_{ij} = \sum_{k=1}^{L^d-1} \frac{1}{\lambda_k} \Psi_i^k \Psi_j^k. \quad (27)$$

Note that since the GF is constructed from the height fluctuations measured from the mean, the zero mode automatically drops out from the sum.

Employing the GF, the average width can be expressed as

$$\langle w^2 \rangle = \left\langle \frac{1}{L^d} \sum_{i=1}^{L^d} (h_i - \bar{h})^2 \right\rangle = \frac{1}{L^d} \sum_{i=1}^{L^d} G_{ii} \quad (28)$$

or, for numerical purposes,

$$\langle w^2 \rangle = \frac{1}{L^d} \sum_{k=1}^{L^d-1} \frac{1}{\lambda_k}. \quad (29)$$

C. Other examples and connections between transport, resistor networks, and the EW synchronization problem

In the network research literature, an ‘‘abstract’’ transport efficiency can be considered in analogy with electric conductance properties of a network [60, 61, 62, 63, 64, 65, 66]. The average resistance of a network gives a simplified but palpable interpretation of its transport properties. If the average network resistance is low, it can be interpreted as a network with good transport properties; if the resistance is high, the network is likely to be a poor choice for transportation purposes.

Consider an arbitrary network with N nodes where the conductance of the link between nodes i and j is A_{ij} . Skipping the details (which can be found in, e.g., Refs. [60, 64, 66]), using Kirchhoff's and Ohm's laws, one can show that the effective two-point resistance of a network can be expressed in terms of the same network propagator (GF) as defined in the previous examples [Eq. (26)],

$$R_{ij} = G_{ii} + G_{jj} - 2G_{ij}. \quad (30)$$

Comparing the above formula to those of the EW process on the same network (and with the same set of $\{A_{ij}\}$), connections between the two different problems can be readily obtained [64, 66]. Calculating the *height-difference* correlation function,

$$\begin{aligned} \langle (h_i - h_j)^2 \rangle &= \left\langle \left((h_i - \bar{h}) - (h_j - \bar{h}) \right)^2 \right\rangle \\ &= G_{ii} + G_{jj} - 2G_{ij} = R_{ij}, \end{aligned} \quad (31)$$

is equivalent to measuring the two-point resistance on the same network. The average resistance (averaged over all pairs of nodes) becomes

$$\bar{R} = \frac{1}{N(N-1)} \sum_{i \neq j} R_{ij} = \frac{2N}{N-1} \langle w^2 \rangle \simeq 2 \langle w^2 \rangle, \quad (32)$$

which is twice the average width for sufficiently large networks [83]. These simple relationships are useful in understanding intuitively how the network topology influences the behavior of different processes in networks. Also, note that the above relationships, Eqs. (31) and

(32), are valid for an arbitrary graph. For networks embedded in a d -dimensional regular grid, such as the one considered in this paper, $N = L^d$. For example, for a one-dimensional chain with unit resistances between each adjacent nodes, the two point resistance is $R_{ij} = |i - j|$, therefore, without any calculations, the height difference correlation function is also $\langle (h_i - h_j)^2 \rangle = |i - j|$.

There is also an extensive literature on the connections between resistor networks (with link conductances A_{ij}) and discrete-time random walks (RW), with *transition probabilities* $P_{ij} = A_{ij} / \sum_k A_{ik}$ from node i to node j [48, 67, 68, 69, 70]. Our results, to be obtained in this paper for the GF on distance-dependent SW networks, hence provide answers for these related problems.

For example, in transport or flow problems on networks, one often considers the ‘‘load’’ of the nodes or the links, which can be captured by an appropriately defined betweenness measure [71, 72, 73] (for a given dynamics). This observable captures the amount of traffic, information, or data, the nodes or the links typically handle in the corresponding information, social, or infrastructure network. For example, in random routing or search problems on complex networks, an appropriate *node betweenness* can be defined as *the expected number of visits* to node i by a random walker (starting at a source node and before reaching its randomly chosen target), averaged over all source and target pairs [74, 75]. It can be shown to be given by [66]

$$b_i = \frac{\sum_k A_{ik}}{2} \bar{R}, \quad (33)$$

where \bar{R} is the average two-point resistance of the associated resistor network with link conductances A_{ij} . The node betweenness can be used to obtain the congestion threshold in queue-limited network traffic [66, 74, 75]. Similarly, one can show that the *link betweenness* b_{ij} for the same RW problem (the expected number of times a walker travels across the link between nodes i and j , averaged over all source and target pairs) can be written as

$$b_{ij} = A_{ij} \bar{R}. \quad (34)$$

The link betweenness, capturing the load of the connections between the nodes, can be used to extract the congestion threshold in bandwidth-limited traffic. Further, one can also show that the average first-passage time for the above random-walk problem (averaged over all source and target pairs) can be written as [69, 70]

$$\bar{\tau} = \frac{\sum_{i,k} A_{ik}}{2} \bar{R}. \quad (35)$$

As all of the above examples illustrate, the average two-point resistance of a graph \bar{R} (or, equivalently, the average steady-state width of the associated EW synchronization landscape) plays a fundamental role in the efficiency of prototypical transport problems.

II. ANNEALED SMALL-WORLD NETWORKS

In the literature of networks the disorder of links is considered *annealed* or *mean-field* (MF) when it can be approximated by its average value. Such a situation can emerge when the process investigated on the network feels only the average effect of the links due to the dynamics of the system, in other words, when the timescale of the changes in the configuration of the links is much shorter than the characteristic timescale of the process on it.

If O is some observable depending on a random potential V , accounting for the effect of the random links, then $[O]^{ann}$ is calculated by replacing V with its expected value:

$$[O(V)]^{ann} = O([V]) \quad (36)$$

Specifically, for the propagator of the diffusion operator, the focus of the present work, one has

$$\begin{aligned} [G_{\mathbf{r}', \mathbf{r}''}]^{ann} &= \left[\left(\frac{1}{\hat{\Delta}^0 + q \hat{\Delta}^{rnd}} \right) \right]_{\mathbf{r}', \mathbf{r}''}^{ann} \\ &= \left(\frac{1}{\hat{\Delta}^0 + q [\hat{\Delta}^{rnd}]_{\mathbf{r}', \mathbf{r}''}} \right)_{\mathbf{r}', \mathbf{r}''}. \end{aligned} \quad (37)$$

Both in the annealed and the quenched case, the ensemble is translationally invariant, and so will be the averages of the observables of the system. $[G_{\mathbf{r}', \mathbf{r}''}]^{ann}$ will only depend on the difference $\mathbf{r}' - \mathbf{r}''$. Let us introduce

$$G^{ann}(\mathbf{r}) = [G_{\mathbf{r}', \mathbf{r}'+\mathbf{r}}]^{ann} \quad (38)$$

where \mathbf{r} is the spatial separation of two sites. Since translationally invariant operators are diagonal in Fourier space, it is useful to calculate the Fourier (or k -space) representation of them. In Fourier space the GF can be written as

$$G^{ann}(\mathbf{k}) = \frac{1}{k^2 + q [\Delta^{rnd}](\mathbf{k})}$$

where k^2 and $[\Delta^{rnd}](\mathbf{k})$ are the Fourier transform of $\hat{\Delta}^0$ and $[\hat{\Delta}^{rnd}]$ respectively. The behavior of $[\hat{\Delta}^{rnd}]$ for $1/L \ll k \ll 1/a$ is calculated in Appendix A, yielding

$$[\Delta^{rnd}](\mathbf{k}) \propto \begin{cases} p & \text{if } \alpha < d \\ pk^{\alpha-d} & \text{if } d < \alpha < d+2 \\ pk^2 & \text{if } d+2 < \alpha \end{cases}, \quad (39)$$

with logarithmic corrections at the boundaries of these different α regimes. In order to keep the treatment of the annealed and the quenched system in parallel, we also call $[\Delta^{rnd}]$ the *annealed self-energy*, $\Sigma^{ann}(\mathbf{r}) = [\Delta^{rnd}](\mathbf{r})$. The real-space behavior can be obtained by inverse Fourier transformation where necessary and, specifically,

$$G^{ann}(\mathbf{0}) = \frac{1}{L^d} \sum_{\mathbf{k} \neq \mathbf{0}} \frac{1}{k^2 + q [\Delta^{rnd}](k)}. \quad (40)$$

In the present and the next sections, the behavior of $G^{ann}(\mathbf{0})$ will be investigated. In Section V, physically measurable quantities will be associated with $G^{ann}(\mathbf{0})$, like the surface width in the EW model and the expected number of returns of random-walk processes.

For calculating scaling properties, we take the continuum limit of these quantities. In this limit, \mathbf{r} is no longer constrained to the lattice sites, so it can point in any direction with the condition $a \leq |\mathbf{r}| \leq L$, the sums replaced by integrals, and Kronecker δ_{ij} by Dirac $\delta(\mathbf{r} - \mathbf{r}')$. To calculate the scaling properties of $G^{ann}(\mathbf{0})$, with respect to p , q , and L , the sum can be approximated with its integral-form limit:

$$G^{ann}(\mathbf{0}) \approx \frac{S_d}{(2\pi)^d} \int_{1/L}^{1/a} \frac{dk k^{d-1}}{k^2 + q [\Delta^{rnd}](k)} . \quad (41)$$

where S_d is the surface of a d -dimensional unit sphere.

Mention must be made that mapping out the different phases of the annealed network is a relatively easy task, and has been investigated by others in other contexts [35, 76].

The results can be summarized as follows.

A. Phase diagram in one dimension

The results for one dimension are sketched in Fig. 2 and the details of the calculations can be found in Appendix B. The relationship of $G^{ann}(0)$ with measurable quantities is explained in more detail in Section V. For $\alpha < 2$, the integral, Eq. (41), converges at both ends, so is system size independent for large L and diverges as $p \rightarrow 0$. There are two regimes, distinguished by their scaling behavior (reflecting on the properties of the underlying random walk/surface): (1) *transient/smooth phase I*, where the system behaves as if the long-range links were uniformly distributed, and $G^{ann}(0)$ is α -independent; (2) *transient/smooth phase II*, where $G^{ann}(0)$ is still finite in the thermodynamic limit, but has an α -dependent divergence as $p \rightarrow 0$. For $\alpha > 2$, $G^{ann}(0)$ has infrared divergence resulting in two system-size dependent regimes: (1) *recurrent/rough phase I*, where the system behaves as if there were no long-range links, and $G^{ann}(0)$ diverges linearly with the system-size, L ; (2) *recurrent/rough phase II*, with sublinear scaling with respect to the system-size. At the boundaries of these phases, logarithmic corrections are present.

B. Phase diagram in two dimensions

The behavior of the annealed two-dimensional system is summarized in Fig. 3. Three different phases are identified: a *logarithmically smooth/transient phase* when $\alpha < 4$, a *doubly-logarithmic rough/recurrent phase* when $\alpha = 4$, and a *logarithmically rough/recurrent phase* when $\alpha > 4$. The details of the calculations can be found in Appendix B.

C. Higher dimensions, $d > 2$

In higher dimensions, the integral Eq. (41) diverges for large k -s but has a well defined cutoff because of the lattice spacing, a . As a result $G^{ann}(0)$ is always finite, which means that the surface is always smooth and the random walker is always transient.

III. QUENCHED SMALL-WORLD NETWORKS

In this section we will develop a perturbation expansion, based on impurity-averaged perturbation theory [77], to calculate the quenched average of the GF over the ensemble of random networks. The reason for investigating such an average is the so-called *self-averaging hypothesis*, that for large enough networks the behavior of the GF, or in general any global quantity, will only deviate slightly from the behavior of its quenched average. This assumption is due to the recognition that if a random system is large enough, the GF samples through a large amount of randomness, which is a large number of random links in our case. In effect, the GF will be the same or very similar from one realization to another and for large enough system sizes it will converge to its quenched value. In principle, this hypothesis can always be checked or proven after setting up a formalism to calculate quenched averages over the randomness. To do so, one has to obtain the quenched variance of the GF. If the variance disappears in the TD limit, the hypothesis is proven to be valid.

For example, the probability distribution of the random walker over the nodes of the network for large times is expected to be self-averaging. One can imagine that after long enough time the random walker will visit a large number of sites, and therefore encounter a large number of random links.

In this section, we will investigate the limit when the density of random links is small ($p \ll 1$). Due their small number, we will treat the diffusion through these random links as perturbation of the d -dimensional diffusion. As a first step, we will consider the ‘‘pedagogical’’ example of a simpler problem, where there is only a single long-range link in the system, which will help us to understand the different terms of the more difficult problem of the perturbation expansion. Second, we will set up a naive perturbation expansion and show the breakdown of it. Third, we will reformulate the expansion to obtain the leading-order behavior of the GF. For special cases, we will obtain higher-order corrections and investigate their behavior.

A. The example of a single link

In this section we will consider two problems that have similar mathematical structure as that of the problem of the quenched network. First, we will calculate the

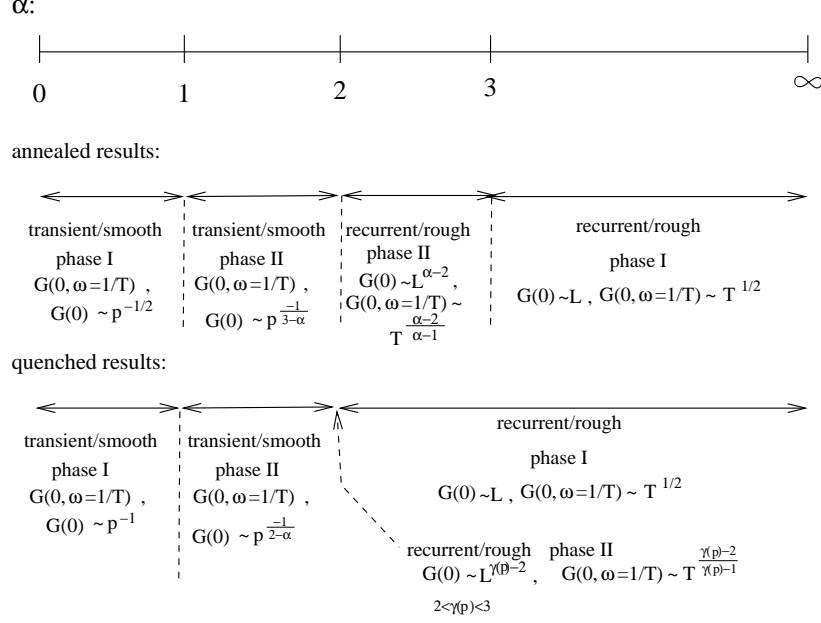
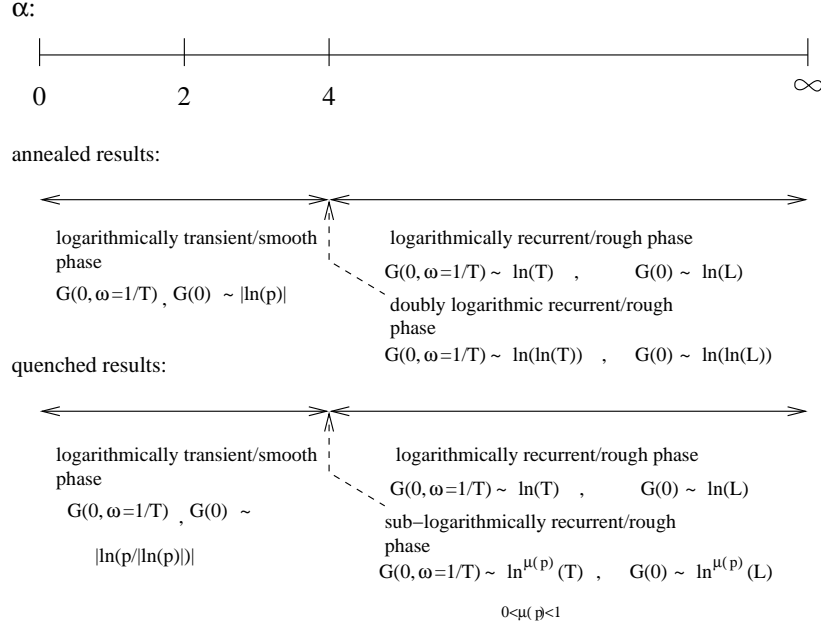


FIG. 2: The one-dimensional phases.

FIG. 3: The two-dimensional phases. (For sake of simplicity, factors of a , the microscopic cutoff, were omitted from the formulas and can be calculated by dimensional analysis.)

Green's function of a diffusion process with a regular d -dimensional diffusion plus a "perturbation" which accounts for particles escaping from the origin with rate q . Second, we will consider the Green's function of a process that will consist of a d -dimensional diffusion plus diffusion between the sites a and b with rate q .

For the first problem, the diffusion operator describing the process is

$$\Gamma = \Delta + qV, \quad (42)$$

where the perturbation to the regular diffusion is $V_{ij} = \delta_{i0}\delta_{0j}$. For this process, the GF can be calculated as

$$G = \frac{1}{\Delta + qV} = \frac{1}{(1 + qVG^0)\Delta} = G^0 - G^0qVG^0 + G^0qVG^0qVG^0 - \dots, \quad (43)$$

where $G^0 = (\Delta^0)^{-1}$ is the GF of the Laplacian on the regular lattice. In Fig. 4 a diagrammatic notation is introduced to represent the above series expansion. Sin-

gle lines, double lines, and crosses denote G^0 , G , and V respectively. Using the specific form of V , G can be calculated as

$$\begin{aligned} G_{ij} &= G_{ij}^0 - G_{i0}^0 q G_{0j}^0 + G_{i0}^0 q G_{00}^0 q G_{0j}^0 \\ &\quad - G_{i0}^0 q G_{00}^0 q G_{00}^0 q G_{0j}^0 + \dots \\ &= G_{ij}^0 - G_{i0}^0 q (1 - q G_{00}^0 + q G_{00}^0 q G_{00}^0 - \dots) G_{0j}^0 \\ &= G_{ij}^0 - G_{i0}^0 \left(\frac{q}{1 + q G_{00}^0} \right) G_{0j}^0 \end{aligned} \quad (44)$$

To have a better grip at what this result means, let us calculate G for one dimension. From Appendix D, $G_{ij}^0 \approx L - |i - j|$. Substituting this to Eqn. (44) and noticing that $\frac{q}{1 + q G_{00}^0} = \frac{q}{((qL)^{-1} + 1)qL} \approx \frac{1}{L} (1 + \frac{1}{qL})$,

$$\begin{aligned} G_{ij} &\approx L - |i - j| - (L - |i|) \frac{1}{L} (1 + \frac{1}{qL}) (L - |j|) \\ &= \frac{1}{q} + |i| + |j| - |i - j|. \end{aligned} \quad (45)$$

Before moving on to the next problem, in the case of this one-dimensional lattice, let us have a closer look at the perturbation expansion of Eq. (44) in light of the exact behavior of the GF, Eq. (45). Comparing the first and the second order term of the perturbation expansion,

$$G_{i0}^0(q) G_{0j}^0 \ll G_{i0}^0(q^2 L) G_{0j}^0. \quad (46)$$

Even though the second order term is higher order in q , it diverges with the system size. As it can be seen from the exact solution, this divergence is not the property of the full GF, G , but that of the ill-defined perturbation expansion. In the next section, a similar problem will be encountered which will be resolved by reordering and resumming the series expansion.

For the second problem, the perturbation is,

$$qV_{ij}^{(a,b)} = q \delta_{ia} \delta_{aj} - q \delta_{ib} \delta_{aj} + q \delta_{ib} \delta_{bj} - q \delta_{ia} \delta_{bj}. \quad (47)$$

The meaning of the first two terms is that particles disappear at node a with rate q and appear at node b . The last two terms are responsible for the inverse process from b to a . In this case we have to solve the same equation, Eq. (43), as before only with a different perturbing potential.

To make the calculation easier, let us rearrange the formula of $V^{(a,b)}$,

$$qV_{ij}^{(a,b)} = q(\delta_{ia} - \delta_{ib})(\delta_{aj} - \delta_{bj}) = q(UW)_{ij}, \quad (48)$$

where we factorized $V^{(a,b)}$ as a product of two matrices $U_{ik} = (\delta_{ia} - \delta_{ib})$ and $W_{kj} = (\delta_{aj} - \delta_{bj})$. This way, the n^{th} ($n > 1$) term of the series expansion of Eq. (43) will become

$$G^0 q U (W G^0 q U)^{n-2} W G^0. \quad (49)$$

The three parts of this expression are $(G^0 U)_{ik} = G_{ia}^0 - G_{ib}^0$, $(W G^0)_{lj} = G_{aj}^0 - G_{bj}^0$, and $(W G^0 U)_{ij} = (\delta_{ak} - \delta_{bk}) G_{kl}^0 (\delta_{la} - \delta_{lb}) = G_{aa}^0 - G_{ab}^0 - G_{ba}^0 + G_{bb}^0 = 2(G_{aa}^0 - G_{ab}^0)$. In the last step, we used the fact that G^0 is symmetric and translationally invariant. Therefore, the n^{th} term in the series expansion is $G_{ik}^0 (\delta_{ka} - \delta_{kb}) q (2q(G_{aa}^0 - G_{ab}^0))^{n-2} (\delta_{al} - \delta_{bl}) G_{lj}^0$. Let us compare it to the n^{th} term of the previous problem: there we had $G_{ik}^0 \delta_{k0} q (q G_{00}^0)^{n-2} \delta_{0l} G_{lj}^0$. As it can be seen, the second problem has the same structure in its expansion as the previous one. The closed form of the GF is

$$G_{ij} = G_{ij}^0 - (G_{ia}^0 - G_{ib}^0) \left(\frac{q}{1 + 2q(G_{aa}^0 - G_{ab}^0)} \right) (G_{aj}^0 - G_{bj}^0). \quad (50)$$

B. From a naive to a self-consistent single-link perturbation expansion

In the case of the random networks, a similar perturbation expansion can be done as in the previous section for a given realization of the random links. The method, Eq. (43), is still valid though in this case the perturbation, V , is more complicated: it consist of a sum of terms like (47) corresponding to the random links in the system. In principle, the GF could be calculated for any long-range-link configuration. Though, such an expression is not really useful for extracting the dependence of the GF on the parameters of the probability distribution of the links.

Averaging over all the realizations will get rid of the details due to the specifics of a given realization and provide us with the dependence on the statistical properties.

Here, a similar diagrammatics will be used as in the previous section in order to keep track of the different terms in the expansion. For the definition of the symbols see Fig. 5.

First, let us take the disorder average, represented by $[\]$, of the perturbation expansion of the GF (see Fig. 5). In this expression, the higher- and higher-order terms have higher- and higher-order moments of the perturbation potential, $\Delta^{r\text{nd}}$. In probability theory, moments

$$\begin{aligned} \underline{\underline{G}} &= \underline{G^0} - \underline{G^0} \underline{qV} \underline{G^0} + \underline{G^0} \underline{qV} \underline{G^0} \underline{qV} \underline{G^0} \\ &\quad - \underline{\quad \times \quad \times \quad \times \quad \quad} + \underline{\quad \times \quad \times \quad \times \quad \times \quad \quad} + \dots \end{aligned}$$

FIG. 4: The simple diagrams of the example of a single link.

$$\begin{aligned} \underline{\underline{G}} &= \underline{\quad \times \quad \times \quad \times \quad \quad} + \underline{\quad \times \quad \times \quad \times \quad \quad} - \underline{\quad \times \quad \times \quad \times \quad \quad} + \dots \\ &= \underline{\quad \times \quad \times \quad \times \quad \quad} + \underline{\quad \times \quad \times \quad \times \quad \quad} + \underline{\quad \times \quad \times \quad \times \quad \quad} \\ &\quad - \underline{\quad \times \quad \times \quad \times \quad \quad} - \underline{\quad \times \quad \times \quad \times \quad \quad} - \underline{\quad \times \quad \times \quad \times \quad \quad} \\ &\quad - \underline{\quad \times \quad \times \quad \times \quad \quad} - \underline{\quad \times \quad \times \quad \times \quad \quad} \\ &\quad + \underline{\quad \times \quad \times \quad \times \quad \quad} + \dots + \underline{\quad \times \quad \times \quad \times \quad \quad} + \dots \end{aligned}$$

FIG. 5: The averaged Green's function in terms of the moments and cumulants of Δ^{rnd} . Single lines, double lines, and crosses denote G^0 , G , and $q\Delta^{rnd}$ respectively. $[\]$ denote the disorder average of an expression with respect to the random potential Δ^{rnd} . Crosses connected by dashed lines represent the cumulant of those random variables (see Fig. 6).

are not really suitable for any type of expansion since higher- and higher-order terms have larger and larger expectational values. Cumulants are more appropriate to describe a random variable since they decay as their order tends to infinity for well behaving PDF-s.

From a diagrammatic point of view, an important property of the cumulants is that the moment of an n^{th} -order scattering is the sum of all the possible combination of cumulants of the n random potentials (see Fig. 6). One might consider this as a recursive definition of the n^{th} -order cumulant in terms of the lower-order cumulants and the n^{th} -order central moment. It is also used to define the self-energy. In the theory of disordered systems, the *self-energy* is a potential added to the unperturbed Hamilton operator and accounts for the average effect of the impurities, i.e. the random links, in the system. The recursive property of the cumulants is also deployed in self-consistent calculations where single lines are substituted with double lines as a result of the recursive resummation of different order single-line diagrams.

$$\begin{aligned} \underline{\quad \times \quad \times \quad \quad} &= \underline{\quad \times \quad \times \quad \quad} + \underline{\quad \times \quad \times \quad \quad} \\ \underline{\quad \times \quad \times \quad \times \quad \quad} &= \underline{\quad \times \quad \times \quad \times \quad \quad} + \underline{\quad \times \quad \times \quad \times \quad \quad} \\ &\quad + \underline{\quad \times \quad \times \quad \times \quad \quad} + \underline{\quad \times \quad \times \quad \times \quad \quad} \\ &\quad + \underline{\quad \times \quad \times \quad \times \quad \quad} \end{aligned}$$

FIG. 6: The second and the third moments in terms of cumulants. The notation is the same as in Fig. 5.

Order of cumulant	Binary distribution	Poisson distribution
1st	p	p
2nd	$p - p^2$	p
3rd	$p - 3p^2 + 2p^3$	p
4th	$p - 7p^2 + 12p^3 - 6p^4$	p
\vdots	\vdots	\vdots

TABLE I: Comparison of the cumulants of the binary and the Poisson distributions with expected value p .

C. Cumulants of the random perturbation potential

In the case of PL-SW networks, the entries of the matrix of the perturbation potential are described by binary PDF-s: there is either a random link between two sites, i and j , is $pf(|i - j|)$ and the probability of having none is $1 - pf(|i - j|)$ (see Eq. (1)). The cumulants of this distribution are shown in Table 3.1.

Observe that all the cumulants are of order p to leading order. The cumulants do not decay as the degree of them increases. Some might think that for PDF-s with such a property an expansion in terms of the cumulants should not work since all terms are of the same order with respect of the expansion parameter, p . Later on in this section we will revisit this question. As for now, let us assume that a cumulant expansion could work in principle.

The random long-range links are independently distributed. Defining

$$x^{(a,b)} = \begin{cases} 1 & \text{with probability } pf(|a - b|) \\ 0 & \text{with probability } 1 - pf(|a - b|), \end{cases} \quad (51)$$

the contribution of each random link to the perturbation potential can be formulated as

$$q\Delta_{ij}^{rnd} = \sum_{a < b} qV_{ij}^{(a,b)} x^{(a,b)}, \quad (52)$$

where $V^{(a,b)}$ is the *single-link* diffusion operator between a and b introduced in the previous section (see Eq. (47)). Therefore, the cumulants are:

$$\begin{aligned}
[q\Delta_{ij}^{rnd}]_c &= \sum_{a<b} qV_{ij}^{(a,b)} [x^{(a,b)}] , \\
[q\Delta_{ij}^{rnd}q\Delta_{kl}^{rnd}]_c &= \sum_{a<b} qV_{ij}^{(a,b)} \sum_{c<d} qV_{kl}^{(c,d)} [x^{(a,b)}x^{(c,d)}]_c \\
&= \sum_{a<b} qV_{ij}^{(a,b)} \sum_{c<d} qV_{kl}^{(c,d)} [(x^{(a,b)})^2]_c \delta_{ac}\delta_{bd} \\
&= \sum_{a<b} q^2 V_{ij}^{(a,b)} V_{kl}^{(a,b)} [(x^{(a,b)})^2]_c , \\
[q\Delta_{ij}^{rnd}q\Delta_{kl}^{rnd}q\Delta_{nm}^{rnd}]_c &= \sum_{a<b} q^3 V_{ij}^{(a,b)} V_{kl}^{(a,b)} V_{nm}^{(a,b)} [(x^{(a,b)})^3]_c . \\
&\vdots
\end{aligned} \tag{53}$$

The n^{th} order cumulant of Δ^{rnd} will be the function of that of $x^{(a,b)}$. To make the analytics slightly easier, let us change the statistical properties of the random networks a little in a way that does not change the behavior of the ensemble in the $p \rightarrow 0$ limit. Instead of binary random variables, as introduced in Eq. (51), Poisson distributed ones will be used with

$$\text{Probability}(x^{(a,b)} = n) = \frac{(pf(|a-b|))^n}{n!} e^{-pf(|a-b|)}. \tag{54}$$

Using Poisson distribution, a negligible fraction of the nodes will have multiple links between them, but this fraction is so small ($O(p^2)$) that it will not affect the average properties of the system. From a mathematical point of view, though, the forms of the cumulants became much simpler

$$[(x^{(a,b)})^n]_c = pf(|a-b|) \tag{55}$$

as it can be seen in Table III C.

Let us have a closer look at the expressions in Eq. (54) and interpret the mathematical formulas. For example, the third order cumulant consist of a sum of terms like $V_{ij}^{(a,b)}V_{kl}^{(a,b)}V_{nm}^{(a,b)}$. Comparing it to the terms of the single-link problem of the previous section, one can see that it corresponds to the 3^{rd} order scattering off a single link between a and b . In general, the n^{th} order cumulant is a sum of n^{th} order single-link scatterings weighted with the expected number of those links, $pf(|a-b|)$.

Using the specific form of $pf(|a-b|)$ and $V^{(a,b)}$ [84], let us calculate the exact form of the different cumulants:

$$\begin{aligned}
q[\Delta_{ij}^{rnd}]_c &= \sum_{a<b} (\delta_{ia} - \delta_{ib})(\delta_{aj} - \delta_{bj}) \frac{p}{\mathcal{N}|a-b|^\alpha} \\
&= \begin{cases} qp & \text{if } i = j \\ -\frac{qp}{\mathcal{N}|i-j|^\alpha} & \text{if } i \neq j, \end{cases} \tag{56}
\end{aligned}$$

i.e. the first cumulant is the annealed ‘‘superdiffusion’’

operator. Note that

$$[\Delta_{ii}^{rnd}]_c = - \sum_{i \neq j} [\Delta_{ij}^{rnd}]_c, \tag{57}$$

namely, the diffusion is ‘‘conservative’’.

For the higher-order cumulants, in order to make it easier to interpret the results, let us have G_{ij} in between the random perturbation operators, as they will appear in the formulas of the following sections (see Section III D),

$$\begin{aligned}
[q\Delta_{ik}^{rnd}G_{kl}q\Delta_{lj}^{rnd}]_c &= \sum_{a<b} (\delta_{ia} - \delta_{ib})(\delta_{ak} - \delta_{bk}) \\
&\times G_{kl}(\delta_{la} - \delta_{lb})(\delta_{aj} - \delta_{bj}) \frac{q^2 p}{\mathcal{N}|a-b|^\alpha} \\
&= \sum_{a<b} (\delta_{ia} - \delta_{ib})(\delta_{aj} - \delta_{bj}) \\
&\times \frac{2(G_{aa} - G_{ab})q^2 p}{\mathcal{N}|a-b|^\alpha}. \tag{58}
\end{aligned}$$

This is also a superdiffusion operator as in the previous case but the weight of the matrix-entries changed to $\frac{2(G_{aa}-G_{ab})q^2 p}{\mathcal{N}|a-b|^\alpha}$. One can easily generalize to the n th order cumulant: If there are n crosses connected by a dashed line, we call these *single-link diagrams*, and when double lines are running in between them, the corresponding matrix is

$$\sum_{a<b} (\delta_{ia} - \delta_{ib})(\delta_{aj} - \delta_{bj}) \frac{(2q(G_{aa} - G_{ab}))^{n-1} qp}{\mathcal{N}|a-b|^\alpha} \tag{59}$$

resulting from the aforementioned properties of multiple scatterings from a single link operator, $V^{(a,b)}$. The generalization to cases when there are different operators in between the cumulants of the perturbation potential is straightforward.

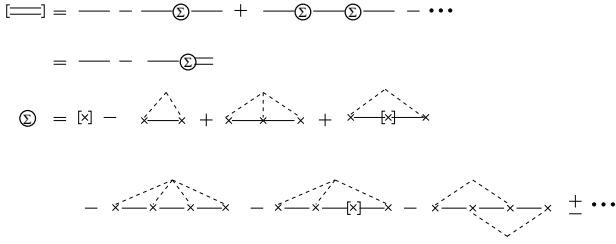


FIG. 7: The introduction of the self-energy, Σ . The notation is the same as in Fig. 5.

D. Introduction of the self-energy, self-consistent resummation of the diagrams

As in quantum field theory, the diagrams of Fig. 5 can be rearranged so that the self-energy is defined. The *self-energy* consist of diagrams that are *irreducible*, i.e. they cannot be cut into two pieces by cutting one of the propagators, G^0 , in them (see Fig 7). In terms of mathematical equations:

$$G = G^0 - G^0 \Sigma G = (\Delta + \Sigma)^{-1}. \quad (60)$$

At this point, let us compare some higher-order diagrams to the first-order one in the self-energy. Let us consider diagrams with n crosses connected by a dashed line and single lines running in between them in one dimension. In this case, $(G_{aa}^0 - G_{ab}^0) \propto r$, where $r = |a - b|$. The contribution of such a diagram to the self-energy is

$$\Sigma_n^{sl}(r) \approx -q^n p \frac{(2r)^{n-1}}{\mathcal{N} r^\alpha} \quad (61)$$

and

$$\begin{aligned} \Sigma_n^{sl}(0) &= \sum_{r \neq 0} \Sigma_n^{sl}(r) \approx q^n p \int_a^L \frac{(2r)^{n-1}}{\mathcal{N} r^\alpha} dr \\ &\propto q^{n-1} p L^{n-1-\alpha} \xrightarrow{L \rightarrow \infty} \infty, \end{aligned} \quad (62)$$

for some large enough n . Just like in the example of a single link, the diagrams diverge with the system size. These divergences can be avoided by including enough intervening scattering events of the propagator between two crosses [77]. In terms of diagrams, it means that a set of diagrams are resummed in between two crosses. If there is a subset of processes with intervening scatterings that will avoid the system-size dependent divergence of the higher-order terms, then resumming over all the possible scattering events between two crosses should also work since it includes those processes too. In terms of diagrams, it means that single lines are replaced by double lines (see Fig. 8). To avoid the overcounting of the diagrams, one must note that, expressing Σ in terms of double lines, some diagrams of Σ with single lines will become “obsolete.” For example, in Fig. 8, there is no double line counterpart of the fourth diagram of Σ in Fig. 7. This is so because such diagrams are already included in the second diagram of Fig. 8. In general, to

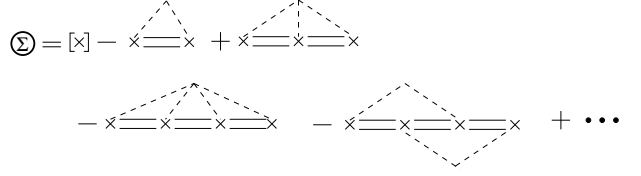


FIG. 8: The self-energy self-consistently. The notation is the same as in Fig. 5.

avoid overcounting, the disallowed diagrams in this expansion of Σ are the ones that can be cut into two by cutting two double lines in them.

In order to have a better idea as to how this resummation happens, let us find all the single-link diagrams that contribute to the second-order self-consistent diagram of Σ in Fig 8. Note that this diagram comes with sign (-1) . The double line between the cumulant of the two scatterings is built of single lines and cumulants of the scatterings between them. Expanding the double line in terms of single lines, diagrams with m scatterings have sign $(-1)^m$ in G . Therefore their contribution to the investigated diagram has sign $(-1)(-1)^m$.

In the single-line expansion of Σ lets consider a subset of diagrams within the $(m+2)^{nd}$ order scatterings. Let this specific subset consist of diagrams which have the second-order cumulant of the first and the last scattering (i.e. the crosses representing them are connected to each other by a dashed line but not to any other crosses) and all the possible combination of cumulants of the intermediate m scattering potentials. Note that these are all parts of the self-energy since they cannot be cut to two by cutting one of the single lines in them. The sign of these diagrams is $(-1)^{(m+1)}$ which agrees with the sign of the m -th order term of G above. Therefore, we found all the single line diagrams that contribute to the m th order term of G in the self-consistent diagram investigated.

The above procedure of replacing single lines with double lines is called *self-consistent perturbation expansion* in the literature of field-theory. Assuming that the expansion works, to obtain the n^{th} order correction to the self-energy one has to calculate the Green’s function using the $(n-1)^{st}$ order approximation of Σ then substitute this GF into the n th order diagram of Σ . In other words, Σ has to be calculated using *successive approximation*.

As done in the single-line case, let us compare the first- and second-order diagrams of the self-energy, denoted by Σ^1 and Σ^2 , to check the validity of this new self-consistent expansion. As long as the higher-order diagrams are higher order in the expansion parameter (p or q) the perturbation expansion works.

Without loss of generality, let us investigate the long-distance behavior of two diagrams: the first-order diagram, the annealed diffusion operator,

$$\Sigma^{(1)}(r) = \frac{qp}{\mathcal{N} r^\alpha}; \quad (63)$$

and the second-order diagram, from Eq. (58),

$$\Sigma^{(2)}(r) = \frac{2(G(0) - G(r))q^2 p}{\mathcal{N}r^\alpha}. \quad (64)$$

Note that, in $\Sigma^2(r)$, $(G(0) - G(r))$ is approximated to first order, i.e. it is calculated with only the first diagram in the self-energy. The details of its calculations are given in Appendix C.

In one dimension, there are four different cases:

1) $\alpha < d$: $(G(0) - G(r)) \propto (pq)^{-\frac{1}{2}}$ and

$$\Sigma^2(r) \propto \frac{1}{r^\alpha} (qp)^{-\frac{1}{2}} pq^2. \quad (65)$$

$\Sigma^2(r) \ll \Sigma^1(r)$ if $q \ll p$. The perturbation expansion can be applied in the weak interaction limit, $q \rightarrow 0$, keeping the number of links fixed, but breaks down in a network with a few but strong long-range links, as $p \rightarrow 0$.

2) $d < \alpha < d + 1$: $(G(0) - G(r)) \propto (pq)^{\frac{-1}{3-\alpha}}$ and

$$\Sigma^2(r) \propto \frac{1}{r^\alpha} (qp)^{\frac{-1}{3-\alpha}} pq^2. \quad (66)$$

$\Sigma^2(r) \ll \Sigma^1(r)$ if $q^{2-\alpha} \ll p$. A similar condition as in case 1) though, here, the strength of the interaction must have a smaller value for the expansion to be applicable.

3) $d + 1 < \alpha < d + 2$: $(G(0) - G(r)) \propto \frac{1}{qp} r^{\alpha-2}$ and

$$\Sigma^2(r) \propto \frac{q}{r^2}. \quad (67)$$

The perturbation expansion breaks down for all parameter values.

4) $d + 2 < \alpha$: The perturbation expansion breaks down. Though, unlike in the cases above, in this regime the effect of the random links is negligible at large distances to that of the regular diffusion on the chain in both the annealed and the quenched system.

In two dimensions there are two cases:

1) $\alpha < d + 2$: $(G(0) - G(r)) \propto -\ln(pqa^2)$. Therefore, the condition for the validity of the perturbation expansion is $q^{-1}e^{-1/q} \ll p$. The perturbation expansion works when $q \rightarrow 0$. In the limit of a small number of strong links, the situation is better than in the one-dimensional cases since the expansion is valid for a large range of p values, but still breaks down in the $p \rightarrow 0$ limit.

2) $d + 2 < \alpha$: Similar to case 4) in one dimension, the perturbation expansion breaks down, though the diffusion through the random links are irrelevant at large distances compared to the regular lattice diffusion.

In three and higher dimensions $(G(0) - G(r)) \propto a^{d-2}$ and

$$\Sigma^2(r) \propto \frac{pq^2 a^{d-2}}{r^\alpha}. \quad (68)$$

The expansion can be applied in the weak interaction limit. In the case of vanishingly small number of links, unlike in the lower-dimensional case, the higher-order terms do not dominate the behavior of the self-energy.

In fact, all the higher-order terms are the same or higher order in p as Σ^1 . The appearance of higher-order diagrams with same p -dependence is due to the fact that the cumulants of Δ^{rnd} are all the same order in p . Though, diagrams with multiple cumulants (see Fig. 9) are of order p^2 . As it will be shown later, the approximation of the first order (annealed) diagram is valid in this case, the perturbation expansion provides the right scaling of the self-energy.

In lower dimensions, $d \leq 2$, the failure of the self-consistent perturbation expansion in terms of the expansion parameter p is due to the fact that diagrams with multiple scatterings off a single link (i.e. diagrams with only one cumulant in them) contribute with the same weight, p , to the self-energy. These scattering processes also contain the GF propagating between two scattering events. The GF is determined from lower order approximations of the self-energy, and therefore is a function of p itself. In the $p \rightarrow 0$ limit, the GF should converge to the original pure GF, G^0 , that is divergent as a function of the system size in these dimensions. Therefore, G is divergent as well when $p \rightarrow 0$. Following this argument, one can understand that the higher-order single-link (or one-cumulant) diagrams dominate the small- p limit behavior of the self-energy since the first-order, single-cross, diagram does not depend on the GF, while all the other single-link diagrams do.

As it was done in Subsection III A, the infinite set of single-link diagrams[85] can be summed. Using Eq. (59),

$$\begin{aligned} \Sigma_{ij}^{sl} &= \sum_{n=1}^{\infty} \sum_{a < b} (\delta_{ia} - \delta_{ib})(\delta_{aj} - \delta_{bj}) \\ &\times \frac{(2q(G_{aa} - G_{ab}))^{n-1} qp}{\mathcal{N}|a-b|^\alpha} \\ &= \sum_{a < b} (\delta_{ia} - \delta_{ib})(\delta_{aj} - \delta_{bj}) \\ &\times \frac{p}{\mathcal{N}|a-b|^\alpha} \frac{q}{1 + 2q(G_{aa} - G_{ab})}. \end{aligned} \quad (69)$$

Since the operator is translationally invariant and the continuum limit is meaningful one can write

$$\Sigma^{sl}(\mathbf{r}) = \frac{-p}{\mathcal{N}r^\alpha} \frac{q}{1 + 2q(G(\mathbf{0}) - G(\mathbf{r}))} \quad (70)$$

Since the self-energy is a conservative (diffusion) operator,

$$\Sigma^{sl}(\mathbf{0}) = - \sum_{\mathbf{r} \neq \mathbf{0}} \Sigma^{sl}(\mathbf{r}). \quad (71)$$

This property can also be derived from Eq. (69). The above pair of equations is referred to as the *Self-Consistent Formula* (SCF).

In order to solve the self-consistent formula, Eq. (70), the following steps are to be taken: First, an *ansatz* has to be made about the large-distance behavior of the self-energy. In most cases, we can make

a very good guess by assuming that the long-distance spatial behavior of the self-energy will be the same as that of the self-energy of the annealed system,

$$\Sigma^{sl}(\mathbf{r}) = \frac{s}{r^\alpha} \propto \Sigma^{an}(\mathbf{r}) = [\Delta^{rnd}] (\mathbf{r}) \quad \text{if } |\mathbf{r}| \gg a, \quad (72)$$

and the strength of the interaction, $s(p, q)$, will be some function of p and q determined by the self-consistent formula.

Second, $(G(\mathbf{0}) - G(\mathbf{r}))$ has to be calculated using the above ansatz, $G(\mathbf{r}) = (\Delta + \Sigma^{sl})^{-1}(\mathbf{r})$. As done before, in order to calculate $G(\mathbf{r})$, the Fourier transforms of the operators are used because of their diagonal form in k -space:

$$G(\mathbf{r}) = \int_{1/L}^{1/a} \frac{e^{i\mathbf{k}\mathbf{r}}}{k^2 + \Sigma(k)} \frac{d^d k}{(2\pi)^d} \quad (73)$$

and

$$(G(\mathbf{0}) - G(\mathbf{r})) = \int_{1/L}^{1/a} \frac{1 - e^{i\mathbf{k}\mathbf{r}}}{k^2 + \Sigma(k)} \frac{d^d k}{(2\pi)^d} \quad (74)$$

The calculation of the scaling of the latter quantity can be found in Appendix C for various forms of $\Sigma(k)$.

Third, the asymptotic form of $(G(\mathbf{0}) - G(\mathbf{r}))$ is substituted into the self-consistent formula [86]. If our ansatz about $\Sigma(\mathbf{r})$ was correct in the first step, the self-consistent formula has to be satisfiable by choosing s appropriately; if it was not correct, a new ansatz has to be made.

Fourth, having Σ^{sl} , $G(0)$ is calculated to obtain physically measurable quantities of the system. The details of the calculations are as follows:

E. The one-dimensional phases

The leading-order results for one dimension are sketched in Fig. 2. Similar phases appear as were predicted by the annealed argument. But, in the transient/smooth phases, we have a different scaling property - a faster divergence as p vanishes. Furthermore, the recurrent/rough phases have different phase-boundaries. Recurrent/rough phase I, where the effect of the long-range links is negligible, spans a wider interval of the α -axis, and recurrent/rough phase II is collapsed to one point on this axis. In this phase, the sublinear behavior of $G(0)$ is no longer determined by the distance-distribution of the random links but rather by their density, p , through Eq. (92). The form of this equation is approximate, but the fact that the exponent μ depends continuously on p is likely to be exact, in light of the scaling arguments in Section IV.

For $0 < \alpha < 1$, let us go through the process step by step. The ansatz, Eq. (72), is $\Sigma(r) = \frac{s}{r^\alpha}$, and its Fourier transform is $\Sigma(k) \approx s$. In the second step, from Appendix C,

$$(G(0) - G(r)) \propto \frac{1}{\sqrt{s}} \quad (75)$$

for large r -s. Substituting this asymptotic form into the SCF, Eq. (70),

$$\frac{s}{r^\alpha} = \frac{p}{\mathcal{N}r^\alpha} \frac{q}{1 + \frac{2q}{\sqrt{s}}} \xrightarrow{s \rightarrow 0} \frac{p\sqrt{s}}{\mathcal{N}r^\alpha}. \quad (76)$$

Therefore

$$s \propto p^2. \quad (77)$$

In the last step we assumed that $s \rightarrow 0$ as $p \rightarrow 0$. This assumption, which is indeed satisfied, can be checked for consistency after obtaining the functional form $s(p)$. In the final step, from Appendix B,

$$G(0) = \int_{1/L}^{1/a} \frac{dk}{k^2 + p^2} \propto p^{-1}. \quad (78)$$

For $3 < \alpha$, the Fourier transform of the ansatz is $\Sigma(k) \propto k^2$. Therefore,

$$(G(0) - G(r)) \propto r. \quad (79)$$

Substituting this in the SCF,

$$\frac{s}{\mathcal{N}r^\alpha} \neq \frac{p}{\mathcal{N}r^\alpha} \frac{1}{r}. \quad (80)$$

The spatial behavior of the two sides of the equation are different, our ansatz does not work. This problem can be fixed easily by setting $\Sigma(r) = \frac{s}{\mathcal{N}r^{\alpha+1}}$. The Fourier transform of any self energy that decays faster than $r^{-(d+2)}$ is $\Sigma(k) \propto k^2$, therefore $(G(\mathbf{0}) - G(\mathbf{r})) \propto r$ is still valid for the new ansatz. Using this new form of $\Sigma(r)$, the self-consistent equation is satisfiable if $s \propto p$. The scaling behavior of the GF is $G(0) \propto L$.

For $1 < \alpha < 2$, the Fourier transform of the ansatz is $\Sigma(k) \propto sk^{\alpha-1}$. Therefore,

$$(G(0) - G(r)) \propto s \frac{-1}{3-\alpha}. \quad (81)$$

Substituting this asymptotic form into the self-consistent formula, $s \propto p^{\frac{3-\alpha}{2-\alpha}}$ and

$$G(0) \propto p^{\frac{-1}{2-\alpha}}. \quad (82)$$

For $2 < \alpha < 3$, the Fourier transform of the ansatz is $\Sigma(k) \propto sk^{\alpha-1}$, which is the same as in the previous case but $G(r)$ has a different long-distance property:

$$(G(0) - G(r)) \propto \frac{1}{s} r^{\alpha-2}. \quad (83)$$

Using this result in the self-consistent formula,

$$\frac{s}{\mathcal{N}r^\alpha} \neq \frac{p}{\mathcal{N}r^\alpha} \frac{s}{r^{\alpha-2}}, \quad (84)$$

A better choice is $\Sigma(r) \propto \frac{s}{r^{\alpha+1}}$. Since $\alpha + 1 > 3$, its Fourier transform is $\Sigma(k) \propto sk^2$, and therefore $(G(0) - G(r)) \propto r$. The SCF is satisfiable if $s \propto p$, resulting in

$$G(0) \propto L. \quad (85)$$

For $\alpha = 2$, the Fourier transform of the ansatz is $\Sigma(k) = k$. Therefore,

$$(G(0) - G(r)) \propto \frac{1}{s} \ln(rs). \quad (86)$$

Substituting into the SCF,

$$\frac{s}{\mathcal{N}r} \neq \frac{p}{\mathcal{N}r} \frac{s}{\ln(rs)}, \quad (87)$$

the two sides have a different r dependence. One iteration step generated a faster decaying function. This tells us that the fixed point of the SCF has to be a function with a faster decay than that of our initial ansatz at long distances. Let us modify the ansatz of Σ , to $\Sigma(r) \propto \frac{s}{nr^\gamma}$, where $2 < \gamma < 3$ and n is a constant factor. For self-energies with such an exponent, $(G(0) - G(r))$ has already been calculated in the $2 < \alpha < 3$ case above. As it will be shown below, in this phase the (γ dependent) constants in $\Sigma(r)$ will have a crucial role in determining the exponent γ .

For this reason one has to calculate the scaling properties of the ansatz of the self-energy with more scrutiny: from Appendix A the result of the Fourier transformation is

$$\Sigma(k) = \frac{s}{n_1} k^{\gamma-1}, \quad (88)$$

where $n_1 = n (2 \sin(\frac{\pi}{2}\gamma) \Gamma(1-\gamma))^{-1}$. Also, from Appendix C, using the above form of the self-energy,

$$(G(0) - G(r)) \approx \frac{n_2}{s} r^{\gamma-2} \quad (89)$$

for large distances, where

$$n_2 = \frac{n \cos(\frac{\pi}{2}\gamma) \Gamma(2-\gamma)}{2\pi \sin(\frac{\pi}{2}\gamma) \Gamma(1-\gamma)} = \frac{n}{2\pi} \cot\left(\frac{\pi}{2}\gamma\right) (1-\gamma). \quad (90)$$

Substituting this into the SCF,

$$\frac{s}{nr^\gamma} = \frac{p}{\mathcal{N}r^2} \frac{s}{n_2 r^{\gamma-2}} = \frac{p s}{\mathcal{N} n_2} \frac{1}{r^\gamma}. \quad (91)$$

The two sides of the equation have the same functional form. Though s is undetermined by the single link approximation, we will see later that some information is still known. The only remaining tunable parameter is γ (in n_2), to equate the two sides of the formula. Noting that $\mathcal{N} = 2 \sum_{i=1}^{\infty} \frac{1}{i^2} = \frac{\pi^2}{3}$, the equation determining the value of γ as a function of p ,

$$1 = p \frac{3}{2\pi} \frac{\tan(\frac{\pi}{2}\gamma)}{\gamma-1}, \quad \text{where } 2 < \gamma < 3 \quad (92)$$

has to be solved for different p -s numerically. Therefore,

$$G(0) \propto \frac{1}{s} L^{\gamma(p)-2}. \quad (93)$$

Note that even though the single-link approximation does not give information about $s(p, q)$, one can still argue about its q dependence: The dimension of s has to be that of $(length)^{\gamma-3}$ since k^2 and $sk^{\gamma-1}$ should have the same dimensions in $G(k)$. Since p is dimensionless for $d = 1$ and $\alpha = 2$, q with dimension $(length)^{-1}$ is the only parameter of the problem that can restore the dimensionality of $\Sigma(k)$. Therefore one may expect that $s(p, q) \propto q^{3-\gamma} f(p)$ where $f(p)$ is undetermined.

F. The two-dimensional phases

The results for the quenched two-dimensional system are summarized in Fig. 3. The overall difference between the annealed and the quenched cases is that the quenched self-energy acquires logarithmic corrections to that of the annealed system. As a result the quenched phases have stronger (or equal) logarithmic divergences than their annealed counterpart. Three different phases are identified: a *logarithmically smooth/transient phase* when $\alpha < 4$, a *sub-logarithmically rough/recurrent phase* when $\alpha = 4$, and a *logarithmically rough/recurrent phase* when $\alpha > 4$. To map the phase space, the single-link self-consistent formula [Eqn. (70)] is used to obtain the leading order behavior of the GF.

The steps of solving the self-consistent formula are the same as in the one-dimensional case. The details are as follows:

For $\alpha < 2$ the Fourier transform of the ansatz is $\Sigma(k) \propto s$. Therefore,

$$(G(\mathbf{0}) - G(\mathbf{r})) \propto \ln(sa^2) \quad (94)$$

and the result of the self-consistent equation as $s \rightarrow 0$ is

$$\frac{p}{\ln s} = s \quad (95)$$

so

$$s \approx \frac{p}{\ln p} + \dots \quad (96)$$

and

$$G(\mathbf{0}) \propto \ln\left(\frac{p}{\ln p}\right). \quad (97)$$

For $2 < \alpha < 4$ the Fourier transform of the ansatz is $\Sigma(k) \propto sk^{\alpha-2}$. Therefore,

$$(G(\mathbf{0}) - G(\mathbf{r})) \propto \ln(sa^{4-\alpha}) \quad (98)$$

and the result of the self-consistent equation is the same as in the previous case: $s \approx \frac{p}{\ln p} + \dots$ and $G(\mathbf{0}) \propto \ln\left(\frac{p}{\ln p}\right)$. For $\alpha > 4$ the Fourier transform of the ansatz is $\Sigma(k) \propto sk^2$. Therefore,

$$\begin{aligned} (G(\mathbf{0}) - G(\mathbf{r})) &= \int_{1/L}^{1/a} \frac{1 - J_0(kr)}{(1+s)k^2} \frac{kdk}{(2\pi)^2} \\ &\propto \int_{1/r}^{1/a} \frac{dk}{k} = \ln(r/a). \end{aligned} \quad (99)$$

Substituting this to the self-consistent formula,

$$\frac{s}{\mathcal{N}r^\alpha} \neq \frac{p}{\mathcal{N}r^\alpha} \frac{1}{\ln(r/a)}. \quad (100)$$

Since the spatial behavior of the two sides of the equation are different, our ansatz does not work. As in the one-dimensional problem, this problem can be fixed by setting $\Sigma(r) = \frac{s}{\mathcal{N}r^\alpha \ln(r/a)}$. The Fourier transform of any self-energy that decays faster than $r^{-(d+2)}$ is $\Sigma(k) \propto k^2$, and therefore $(G(\mathbf{0}) - G(\mathbf{r})) \propto \ln(r/a)$ is still valid for the new ansatz. Using this new form of $\Sigma(r)$, the self-consistent equation is satisfied if $s \approx p$. The scaling behavior of the GF is

$$G(\mathbf{0}) \propto \ln L. \quad (101)$$

For $\alpha = 4$, let us look into the details. In real space, $\Sigma(\mathbf{r}) = \frac{s}{\mathcal{N}r^4}$, and its Fourier transform is $\Sigma(k) = sk^2 \ln(ka)$ (see the calculations of Appendix A). Therefore, from Appendix C,

$$(G(\mathbf{0}) - G(\mathbf{r})) \propto \frac{1}{s} \ln(s \ln(r/a)). \quad (102)$$

Substituting the above result into the self-consistent equation,

$$\frac{s}{r^4} \neq \frac{p}{\mathcal{N}r^4} \frac{s}{\ln(s \ln(r/a))}. \quad (103)$$

The two sides of the equation do not match because the iteration process generated a double-logarithmically stronger decay of the self-energy. If one tried another ansatz, $\Sigma(r) \propto \frac{1}{r^{4+\epsilon}}$, $\epsilon \ll 1$, the iteration step would weaken the decay making it $\propto \frac{1}{r^4 \ln(r/a)}$. Therefore the fixed point of the self-consistent equation for $\alpha = 4$ should be a function with a decay between $\frac{1}{r^4}$ and $\frac{1}{r^{4+\epsilon}}$. After some guess work, a better ansatz is

$$\Sigma(\mathbf{r}) = \frac{s}{n r^4 \ln^\mu(r/a)}, \quad (104)$$

where $0 > \mu > 1$ and n is a constant. Its Fourier space behavior from Appendix A for small k -s is

$$\Sigma(k) \propto \frac{sc_1(\mu)}{n} k^2 \ln^{1-\mu}(ka) + \mathcal{O}\left(\frac{k^2}{\ln^\mu(ka)}\right), \quad (105)$$

where $c_1(\mu)$ is a constant, the result of the Fourier transformation. From Appendix C

$$G(\mathbf{0}) - G(\mathbf{r}) \propto \frac{n c_2(\mu)}{s c_1(\mu)} \ln^\mu(r/a) + \mathcal{O}(\ln^{\mu-1}(r/a)), \quad (106)$$

where $c_2(\mu)$ is a constant, the result of the inverse-Fourier transformation. Substituting this result to the self-consistent formula when $r \rightarrow \infty$,

$$\frac{s}{n r^4 \ln^\mu(r/a)} = \frac{p}{\mathcal{N}r^4} \times \frac{n c_2(\mu)}{s c_1(\mu)} \times \frac{1}{\ln^\mu(r/a)} \quad (107)$$

yielding

$$1 = \frac{p}{\mathcal{N}} \times \frac{c_1(\mu)}{c_2(\mu)}. \quad (108)$$

where $\mathcal{N} = \sum_{\mathbf{r}} \frac{1}{r^4}$ is the normalization constant of the probability distribution of the random links, and $c_1(\mu)$ and $c_2(\mu)$ are constants defined by the Fourier transformation of specific functions. As in the one-dimensional case, μ became a continuously varying function of p , defined by Eq. (108). Though, in this calculation, c_1 and c_2 are not determined, in future research one may try to perform the Fourier transformations more accurately or determine their value numerically by performing discrete-Fourier transformation.

Finally, one finds

$$G(0) \approx \int_{1/L}^{1/a} \frac{kdk}{k^2 + sk^2 \ln^{1-\mu}(ka)} \quad (109)$$

$$\propto \frac{1}{s} \ln^{\mu(p)}(L), \quad 0 < \mu(p) < 1, \quad (110)$$

a “*sub-logarithmic*” divergence with the system-size.

From numerical and experimental point of view, one must note that the above logarithmic differences are difficult to measure.

G. Higher dimensions, $d \geq 3$

In the naive perturbation expansion it was seen that higher-order single-link diagrams give the same order contribution in p as the first order one. From the SCF, one can verify this result since the GF is finite and determined by its behavior at the lattice scale (see Appendix C),

$$(G(\mathbf{0}) - G(\mathbf{r})) \approx g \propto a^{d-2}, \quad (111)$$

where g is some constant and the exact value of it is determined by the microscopic details of the lattice. Substituting this into the SCF,

$$\Sigma^{sl}(r) = \frac{p}{\mathcal{N}r^\alpha} \frac{q}{1 + 2qg} \quad (112)$$

and $G(0)$ is independent of p and q to leading order, $G(0) \approx g + \dots$

H. Higher-order corrections

In the previous sections the self-energy was approximated with the infinite sum of single-link diagrams. Here, the contribution of higher-order diagrams is investigated in the case of the plain SW network ($\alpha = 0$) and the other cases, $\alpha \neq 0$, are left to future research. The first such diagram is that of Fig. 9(a), the lowest-order two-cumulant diagram. It is called a two-cumulant diagram since it has two sets of crosses: in each set, crosses

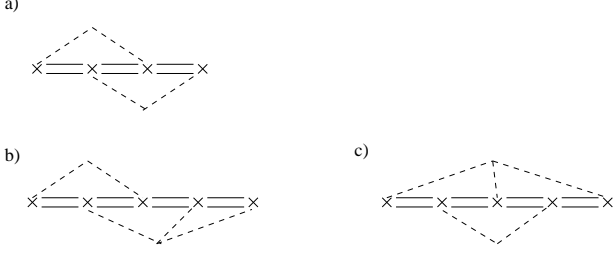


FIG. 9: Two cumulant diagrams. The notation is the same as in Fig. 5. Moreover, square brackets, $[\]$ were dropped from around double lines for the sake of clarity.

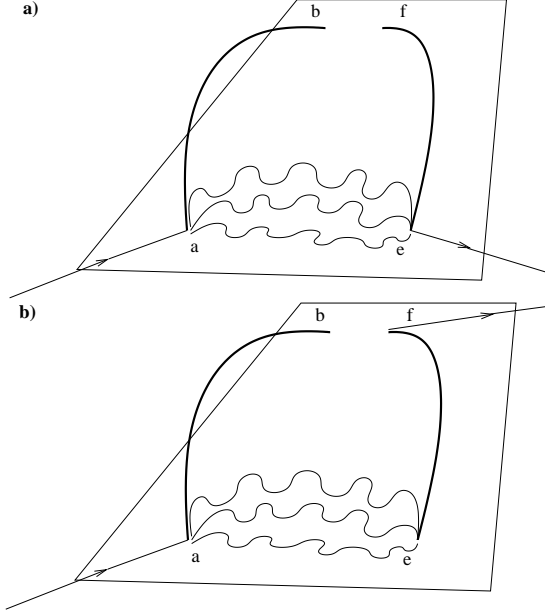


FIG. 10: Sketch of the leading order processes in the two-cumulant diagram of Fig. 9(a). Links are represented by fat lines, GF-s are represented by wavy lines, and the underlying d -dimensional lattice is represented by a flat sheet. The two indices of the corresponding matrix are represented by straight lines with an arrow. a) the leading order process at short distances; (b) the leading order process at long distances.

are connected to each other by dashed line. According to the definition of the diagrams, these sets correspond to separate cumulants of the perturbation potential.

In terms of matrices the corresponding scattering potential is

$$\begin{aligned}
 \Sigma^{2c} &= q^4 \sum_{a,b,e,f} V^{(a,b)} G V^{(e,f)} G V^{(a,b)} G V^{(e,f)} \\
 &\times [(x^{(a,b)})^2] [(x^{(e,f)})^2] \\
 &= q^4 \frac{p^2}{L^{2d}} \sum_{a,b,e,f} V^{(a,b)} G V^{(e,f)} G V^{(a,b)} G V^{(e,f)},
 \end{aligned} \tag{113}$$

where the indices of the matrices were dropped for the

sake of simplicity and $[(x^{(e,f)})^n] = p/L^d$ for plain SW networks. Note that each operator in the sum is conservative [see Eq. (57)] hence the whole diagram is so too. Let us investigate a single term of this sum. Using Eq. (48), the factorized form of $V^{(a,b)}$ and $V^{(e,f)}$, one can see that such a term consist of three scatterings of the GF back and forth between two links in the system: a link between a and b and an other one between e and f . All the possible combinations of scatterings between the links are present. It can be shown and we will see it in an example that the most important terms in the sum are such where all the three GF-s in the diagram scatter between the same legs of the links, let us say between a and e . At small distances, the most important process of them is when the process starts with scattering off a then the GF scatters between a and e three times and finally it “scatters out” at e (see Fig. 10(a)). The matrix corresponding to this process is

$$\begin{aligned}
 \Sigma_{ij}^{2c,A} &= q^4 \frac{p^2}{L^{2d}} \sum_{a,e} \sum_{b,f} \delta_{ia} (G_{ae})^3 \delta_{ej} \\
 &= q^4 \frac{p^2}{L^{2d}} L^d L^d \sum_{a,e} \delta_{ia} (G_{ae})^3 \delta_{ej} \\
 &= (G_{ij})^3 q^4 p^2.
 \end{aligned} \tag{114}$$

At large distances the main contribution comes from a process depicted in Fig. 10(b) [87]. It starts off exactly the same as in the previous case but in the final step the particle jumps over the long-range link between e and f and scatters out at f . The corresponding matrix is

$$\begin{aligned}
 \Sigma_{ij}^{2c,B} &= -q^4 \frac{p^2}{L^{2d}} \sum_{a,f} \sum_{b,e} \delta_{ia} (G_{ae})^3 \delta_{fj} \\
 &= -\sum_{a,f} \delta_{ia} \delta_{fj} q^4 \frac{p^2}{L^{2d}} \sum_b \sum_e (G_{ae})^3 \\
 &= -q^4 \frac{p^2}{L^d} \sum_e (G_{ie})^3.
 \end{aligned} \tag{115}$$

Note that these two processes are not conservative, yet the sum of them is, which is required for the self-energy. In summary, in the continuum limit,

$$\Sigma^{2c,A+B}(r) = q^4 p^2 \left(G(r)^3 - \frac{1}{L^d} \int G(r')^3 d^d r' \right). \tag{116}$$

Note that for long distances

$$\Sigma^{2c}(r) \approx -q^4 \frac{p^2}{L^d} \int G(r')^3 d^d r', \tag{117}$$

the diagram is distance independent and uniform, and the contribution of it is a mean-field interaction just like the contribution of the leading order terms but with a different strength.

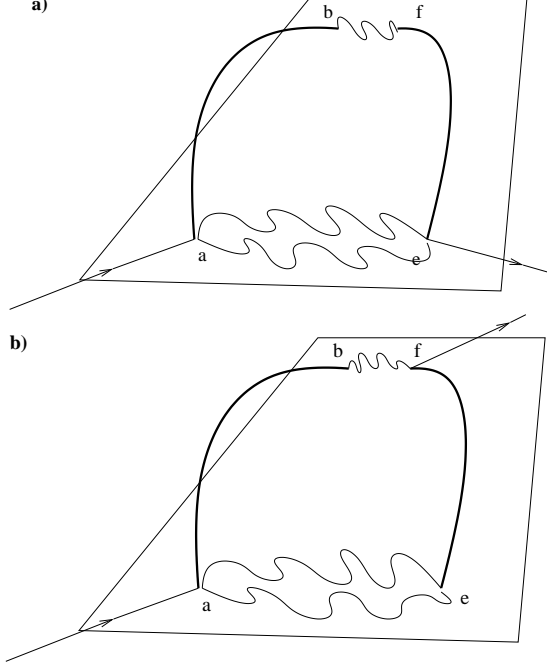


FIG. 11: Sketch of a process the contribution of which vanishes in the thermodynamic limit compared to the leading order one, depicted in Fig. 10.

As an example, let us investigate another term in the diagram, where not all the GF scatter between the same legs of the two links, and see that the contribution of such a diagram is vanishing in the large system size limit. This process starts with scattering off a . The GF then propagates back and forth between a and e twice before it jumps over the long-range link between a and b , where it then propagates from b to f , and finally jumps from f to e (see Fig. 11(a)). The corresponding matrix, up to combinatorial factors, is

$$\begin{aligned}\Sigma_{ij}^{2c,C} &= q^4 \frac{p^2}{L^{2d}} \sum_{a,e} \delta_{ia} \delta_{ej} (G_{ae})^2 \sum_b \sum_f G_{bf} \\ &= (G_{ij})^2 q^4 \frac{p^2}{L^d} \sum_f G_{bf}\end{aligned}\quad (118)$$

and the long-distance counter-term of it is [see Fig. 11(b)]

$$\Sigma_{ij}^{2c,D} = -q^4 \frac{p^2}{L^{2d}} \sum_f (G_{af})^2 \sum_b G_{be}.\quad (119)$$

In the continuum limit

$$\begin{aligned}\Sigma^{2c,C+D}(r) &= q^4 \frac{p^2}{L^d} \left(G(r)^2 \int G(r') d^d r' \right. \\ &\quad \left. - \frac{1}{L^d} \int G(r')^2 d^d r' \int G(r'') d^d r'' \right).\end{aligned}\quad (120)$$

Compared to the leading order term, $\Sigma^{2c,A+B}(r)$, this matrix vanishes in the thermodynamic limit.

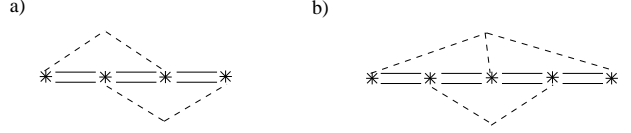


FIG. 12: Resummed two-cumulant diagrams. Stars represent the resummed scattering potentials introduced in Sect. III H. Otherwise, the notation is the same as in Fig. 5. Square brackets, $[\]$ were dropped from around double lines for the sake of clarity.

Qualitatively, the above result can be understood from the following argument: For the process depicted in Fig. 10, only two endpoints, a and e , of the two links have to be within a distance proportional to the correlation length of G of each other so the GF can propagate with finite weight between them. For the process of Fig. 11, both endpoints of both links have to be within a distance of the correlation length from each other, a close to e and b close to f . Since the two links are randomly spread on the lattice in a uniform fashion, having both endpoints of both links in the vicinity of each other is much less likely than having only one endpoint of one link close to one endpoint of the other link.

In low dimensions, some higher-order two-link diagrams have the same problem as the higher-order single-link diagrams. For single-link diagrams, it was demonstrated that the second-order diagram was more dominant than the first-order one in the $p \rightarrow 0$ limit. There are two-link (or two-cumulant) diagrams that involve GF-s propagating between the endpoints of the same link, just like in the case of single-link diagrams. For example, the last double line of Fig 9(b) represents such an event (it can be checked by expressing the diagram in terms of matrices). Such a GF will have a contribution to the diagram which is divergent as $p \rightarrow 0$. Since this divergent contribution is the only difference between this diagram and the diagram in Fig. 9(a), the higher-order diagrams will dominate the small p behavior. As it was done before, this problem can be avoided by resumming over all the single-link scatterings of such diagrams. As a result, when there is a scattering off a link, the scattering is substituted by all the single link scatterings. In terms of matrices the substitution

$$\begin{aligned}qV^{(ab)} &\rightarrow qV^{(ab)} - qV^{(ab)}GqV^{(ab)} \\ &\quad + qV^{(ab)}GqV^{(ab)}GqV^{(ab)} - \dots\end{aligned}\quad (121)$$

is made for all \times -es in the diagrams. It is known from the single-link calculations that the above infinite sum yields

$$V^{(ab)} \frac{q}{1 + 2q(G_{aa} - G_{ab})}.\quad (122)$$

One can say that the result of the resummation is that the strength of the interaction gets *renormalized* from q to $\frac{q}{1+2q(G_{aa}-G_{ab})}$.

In a typical situation the separation of a and b diverges with the system size. Therefore, in such situations, G_{ab} is

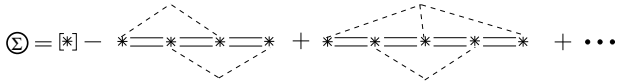


FIG. 13: The self-energy in terms of the resummed potentials. The notation is the same as in the previous figure.

vanishingly small because the GF has a finite correlation length. As a result, the resummed scattering potential can be well approximated by

$$V^{(ab)} \frac{q}{1 + 2qG(0)} \quad (123)$$

in the continuum limit. In diagrammatic notation, the above resummation is represented by replacing the crosses with stars as shown in Fig. 12. The expansion of the self-energy in terms of the resummed potentials is shown in Fig. 13.

Using these renormalized single-link scattering potential, let us calculate the leading order behavior of the diagram in Fig. 12(a). The calculation is the same as was done for the diagram of Fig. 9(a) except that q is replaced by $\frac{q}{1+2qG(0)}$ in Eq. (116).

In one dimension, $G(0) \propto p^{-1}$. In the limit $p \rightarrow 0$,

$$\frac{q}{1 + 2qG(0)} \rightarrow p. \quad (124)$$

Therefore, the second-order term in the resummed self-energy scales as

$$\Sigma^{2c}(r) \propto -\frac{p^4 p^2}{L} \int G(r')^3 dr' \quad (125)$$

at large distances. The integral in the expression can be approximated using the results of Appendix D,

$$G(r) \propto \begin{cases} s^{-1/2} & \text{if } r \ll \xi \\ 0 & \text{if } r \gg \xi \end{cases} \quad (126)$$

where $s \propto p^2$, obtained from the single-link approximation [see Eq. (77)], and $\xi = s^{-1/2}$ is the correlation length as before. Therefore

$$\int G(r')^3 dr' \propto p^{-4} \quad (127)$$

and

$$\Sigma^{2c}(r) \propto \frac{p^2}{L}. \quad (128)$$

The Fourier transform of this operator for small wavenumbers $\Sigma^{2c}(k) \propto p^2$ has the same p dependence as the leading order one, Eq. (77). Higher-order diagrams, like the one in Fig. 12(b), yield contributions of the same order, p^2 . As a result, it can be concluded that the self-energy scales as p^2 for small p -s, though neither the coefficient of it nor higher-order corrections are known.

In two dimensions, $G(0) \propto \ln p$ from Eq. (97), therefore q is renormalized to $1/\ln p$. The second-order correction to the self-energy at large distances

$$\Sigma^{2c}(r) \propto -\frac{p^2}{(\ln p)^4 L^2} \int G(r')^3 d^2 r'. \quad (129)$$

From Appendix D, the integral can be approximated using

$$G(r) \propto \begin{cases} \text{const.} + \ln(r/\xi) & \text{if } r \ll \xi \\ 0 & \text{if } r \gg \xi \end{cases} \quad (130)$$

where $\xi = s^{-1/2} \propto \sqrt{\ln p/p}$ from Eq. (96). Therefore,

$$\int G(r')^3 r' dr' \propto \frac{\ln p}{p} \quad (131)$$

and

$$\Sigma^{2c}(r) \propto \frac{p}{(\ln p)^3 L^2}. \quad (132)$$

In Fourier space, as $p \rightarrow 0$, $\Sigma^{2c}(k) \propto p/(\ln p)^3 \ll \Sigma^{sl}(k) \propto p/\ln p$.

In conclusion, in two dimensions, the single-link perturbation expansion of Fig. 13 works. The mean-field model acquires logarithmic corrections from sample-to-sample fluctuations. The fact that the perturbation expansion works in two dimensions raises the possibility of an ϵ -expansion for $d = 2 - \epsilon$ which was studied in [23]. For small ϵ -s, it was shown that the higher-order diagrams of the perturbation expansion produce higher-order terms in ϵ . Though $\epsilon = 1$ for $d = 1$, the ϵ expansion still defines an ordering of the diagrams making it possible to obtain more accurate analytic predictions for the behavior of the system in the $p \rightarrow 0$ limit.

IV. SCALING ARGUMENTS

After the more careful perturbative treatment of the previous section, let us revisit the effect of long range links and estimate the behavior of the quenched system using scaling and renormalization arguments.

A. Estimating the validity of the annealed approximation

In many statistical systems introducing random long-range links to the underlying lattice results in mean-field (MF) or, in our terminology, annealed behavior [38]. In the following, we will study the self-consistency of the annealed approximation by estimating the sample-to-sample fluctuations of the quenched systems around it [78] [88].

First, we consider the plain SW network ($\alpha = 0$). For this estimation, we utilize the EW Hamiltonian [Eq. (25)]

expressed in terms of the random component of the adjacency matrix, $A_{\mathbf{r},\mathbf{r}'}$, and the difference of the fields at site \mathbf{r} and \mathbf{r}' :

$$\begin{aligned} H[\vec{h}] &= H_0[\vec{h}] + q \sum_{\mathbf{r},\mathbf{r}'} A_{\mathbf{r},\mathbf{r}'} (h_{\mathbf{r}} - h_{\mathbf{r}'})^2 \\ &= H_0[\vec{h}] + q \sum_{\mathbf{r},\mathbf{r}'} [A_{\mathbf{r},\mathbf{r}'}] (h_{\mathbf{r}} - h_{\mathbf{r}'})^2 \\ &\quad + q \sum_{\mathbf{r},\mathbf{r}'} (A_{\mathbf{r},\mathbf{r}'} - [A_{\mathbf{r},\mathbf{r}'}]) (h_{\mathbf{r}} - h_{\mathbf{r}'})^2 \\ &= H_0[\vec{h}] + [H^{rnd}] [\vec{h}] + H_{fluct.}^{rnd} [\vec{h}], \end{aligned} \quad (133)$$

where H_0 is the Hamiltonian of the EW model on the regular, unperturbed, lattice and H^{rnd} is the ‘‘energy’’ due to the random part of the network.

According to MF theory, the last term in H ,

$$q \sum_{\mathbf{r},\mathbf{r}'} (A_{\mathbf{r},\mathbf{r}'} - [A_{\mathbf{r},\mathbf{r}'}]) (h_{\mathbf{r}} - h_{\mathbf{r}'})^2 \quad (134)$$

is negligible compared to the second one because the sample-to-sample fluctuations of $A_{\mathbf{r},\mathbf{r}'}$ are suppressed due to averaging over a large number of sites. For a link between two sites, the relative size of these fluctuations can be quantified by

$$\frac{\sqrt{[(A_{\mathbf{r},\mathbf{r}'})^2] - [A_{\mathbf{r},\mathbf{r}'}]^2}}{[A_{\mathbf{r},\mathbf{r}'}]}, \quad (135)$$

the ratio between the standard deviation and the mean of the random potential.

For the whole system, one has to average over many sites to estimate the magnitude of the fluctuations in the energy, $H[\vec{h}]$. Averaging over the entire system would suppress the fluctuations, though doing so would underestimate their strength. This can be understood in the following argument:

If the separation of \mathbf{r} and \mathbf{r}' is less than the correlation length, ξ , of the field $h_{\mathbf{r}}$, the values of the field at those two sites are close to each other, and $(h_{\mathbf{r}} - h_{\mathbf{r}'})^2$ is small. Therefore, most of the contribution to the energy comes from sites where \mathbf{r}' is outside of the correlation volume of the field at site \mathbf{r} .

On the other hand, the fluctuations in the energy will only amplify the effect of each other where the values of the field are correlated, i.e. over volumes $\propto \xi^d$. Therefore, the condition for the MF or annealed approximation to be valid is

$$\frac{\sqrt{\int_{|\mathbf{r}|<\xi} \int_{\xi<|\mathbf{r}-\mathbf{r}'|} d^d r \int d^d r' ((A_{\mathbf{r},\mathbf{r}'})^2) - [A_{\mathbf{r},\mathbf{r}'}]^2}}{\int_{|\mathbf{r}|<\xi} \int_{\xi<|\mathbf{r}-\mathbf{r}'|} d^d r \int d^d r' [A_{\mathbf{r},\mathbf{r}'}]} \ll 1. \quad (136)$$

Here, we used the fact that the standard deviation of a sum of random variables is the square root of the sum of their variances. From Subsection III C, $[A_{\mathbf{r},\mathbf{r}'}] = ((A_{\mathbf{r},\mathbf{r}'})^2) - [A_{\mathbf{r},\mathbf{r}'}]^2 = p/L^d$ and the correlation length

is $\xi \propto (pq)^{-1/2}$. The above condition can be expressed as

$$p^{-1+d/2} q^{d/2} \ll 1. \quad (137)$$

The assumptions of the MF approximation are always valid when $q \rightarrow 0$. In one dimension, if $p \ll q$, the sample-to-sample fluctuations destroy the MF behavior otherwise MF approximation can still be applied. In two dimensions, if $p \rightarrow 0$ the MF predictions acquire logarithmic corrections from the sample-to-sample fluctuations (see Section III F). In three dimensions and above, the MF criterion is always satisfied.

Second, when $\alpha < d$, $[H^{rnd}]$ generates a mass (or finite correlation length) just like in the case of a plain SW network and $\xi \propto (pq)^{-1/2}$ as well. The same argument can be repeated as in the previous case. The condition of the MF behavior, Eq. (136), is

$$p^{-1+d/2} q^{d/2} \ll 1. \quad (138)$$

Third, when $d < \alpha < d + 2$, strictly speaking, there is no correlation length in the system, though the typical size of correlations is proportional to l_{\times} , defined by the lengthscale above which the long-range random links dominate the behavior of the system. In Fourier space,

$$k_{\times}^2 = pq k_{\times}^{\alpha-d}, \quad (139)$$

where $k_{\times} = l_{\times}^{-1}$. Thus, for the lengthscale l_{\times} one finds $l_{\times} = (pq)^{-\frac{1}{2+\alpha-d}}$. Repeating the same argument as above, replacing the role of ξ by l_{\times} , and using $[A_{\mathbf{r},\mathbf{r}'}] = ((A_{\mathbf{r},\mathbf{r}'})^2) - [A_{\mathbf{r},\mathbf{r}'}]^2 = p/(\mathcal{N}r^{\alpha})$, one arrives at the condition

$$p^{d-2} q^{2d-\alpha} \ll 1 \quad (140)$$

for the MF approximation to be valid. Observe that in one dimension, if $2 < \alpha < 3$, the MF approximation breaks down for all p -s and q -s. In all the other cases the condition is similar to those of the plain SW network, but due to the distance-dependent cutoff of the links, a higher density of long-range links is required for the MF approximation to be valid (i.e. p has to be larger for observing MF behavior).

Fourth, when $d + 2 < \alpha$, the typical size of the correlations is that of the system size, so one cannot apply the above argument. Though, one can introduce a ‘‘virtual’’ correlation length to the system, $\xi_{\mathbf{v}}$, check the condition of the MF approximation, Eq. (136), as a function of $\xi_{\mathbf{v}}$, and in the final step take the limit when the correlation length goes to infinity (or, at least, to the system-size). The result is

$$p^{-1} \xi_{\mathbf{v}}^{(\alpha-2d)} \ll 1. \quad (141)$$

In conclusion: For $d + 2 < \alpha < 2d$, the condition for the MF approximation is satisfied since $\xi_{\mathbf{v}}^{(\alpha-2d)} \rightarrow 0$ as $\xi_{\mathbf{v}} \rightarrow \infty$. For $2d < \alpha$, the condition of for the MF condition is not satisfied since $\xi_{\mathbf{v}}^{(\alpha-2d)} \rightarrow \infty$ as $\xi_{\mathbf{v}} \rightarrow \infty$.

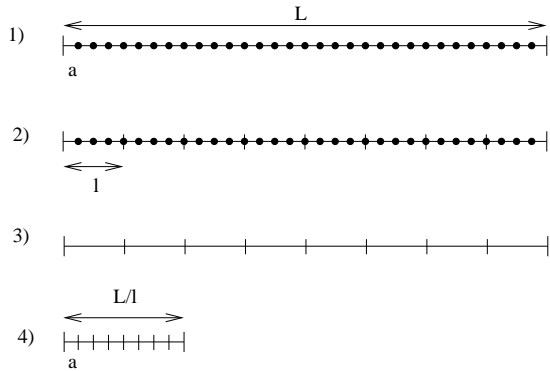


FIG. 14: The steps of the renormalization procedure: 1) Take the original system. 2) Divide it into boxes of size l . 3) Average over the behavior within each l -sized box. 4) Rescale the system so that $l \rightarrow a$.

B. Renormalization

As it was shown above, MF theory is insufficient to describe diffusive processes on quenched SW networks for certain parameter regimes. Though, renormalization approach can capture the universal behavior of these systems: Assuming that the large scale properties of the system are not influenced by the microscopic details, one can average over the small lengthscale behavior according to the steps of Fig. 14.

In the following, we will investigate how the diffusion operator changes doing the steps of renormalization. Diffusion on PL-SW networks is described only by two parameters: p and q (besides d , the dimensionality of the system). First, the change of the density of random links under a change in scale is considered. Second, we will look at the renormalization of q for only a single link in the system. Third, we will combine the results at hand to calculate the scaling of the GF on a PL-SW network; since such a network includes many links, we will have to include interaction between links when the density of links becomes of order unity at the given scale.

C. Renormalization of p

As defined in the Introduction, p is the probability of a site having a random link emanating out of that site irrespective of where the link ends. The first two steps of the renormalization procedure are straightforward. In the third step, after averaging over a cell of size $(al)^d$ the probability of a node within the cell to have a random link pointing outside of that cell is $\int_{al}^L p \frac{r^{d-1} dr}{N r^\alpha}$. For all the nodes within the cell, this probability is

$$\tilde{p} = l^d \int_{al}^L p \frac{r^{d-1} dr}{N r^\alpha} \propto l^d p \times \begin{cases} \frac{L^{d-\alpha}}{N} & \text{if } \alpha < d \\ \frac{(al)^{d-\alpha}}{N} & \text{if } d < \alpha \end{cases} \quad (142)$$

where the normalization constant is

$$\mathcal{N} = \sum_{\mathbf{r}} \frac{1}{r^\alpha} \propto \int_a^L \frac{r^{d-1} dr}{r^\alpha} \approx \begin{cases} L^{d-\alpha} & \text{if } \alpha < d \\ a^{d-\alpha} & \text{if } d < \alpha \end{cases} \quad (143)$$

Therefore,

$$\tilde{p} \propto p \times \begin{cases} l^d & \text{if } \alpha < d \\ l^{2d-\alpha} & \text{if } d < \alpha. \end{cases} \quad (144)$$

In the fourth step, the $(al)^d$ sized cell is rescaled to size a^d and the probability of one such node to have a random link will be that of the original cell, $(al)^d$. In summary, the flow equation of the parameter of the probability distribution of the random links is

$$p \rightarrow \tilde{p} \propto p \times \begin{cases} l^d & \text{if } \alpha < d \\ l^{2d-\alpha} & \text{if } d < \alpha. \end{cases} \quad (145)$$

D. Renormalization of q for a single sink and a single link

In renormalization group theory, the procedure to obtain the universal long-wavelength properties of the system is averaging over short wavelength modes. Due to interactions which mix long and short wavelength modes, the Hamiltonian that describes the statistical properties of the system will change: these mixing interactions will generate modified or new interactions between long wavelength modes after averaging.

Let us follow through this procedure in the case of when there is only a single sink in the system. The Hamilton operator of the system is $H = H^0 + qV$. The unperturbed Hamiltonian is the diffusion operator, $H_{kk'}^0 = \delta_{kk'} k^2$ in Fourier space. The perturbation potential is $qV_{ij} = q\delta_{i0}\delta_{0j}$ in real space and

$$qV_{kk'} = \frac{q}{L^d} \quad (146)$$

a “uniform” matrix in Fourier space. We will distinguish between long and short wavelength modes

$$\Phi_k = \begin{cases} \Phi'_k & \text{if } k < 1/l \\ \Phi''_k & \text{if } k > 1/l. \end{cases} \quad (147)$$

Making this distinction, let us introduce the following division of V in Fourier basis:

$$V = \begin{pmatrix} V_1 & V_A \\ V_B & V_2 \end{pmatrix}, \quad (148)$$

where V_1 and V_2 act on the long and short wavelength modes and V_A and V_B are mixing between them. The Laplace operator is divided likewise:

$$H^0 = \begin{pmatrix} H_1 & 0 \\ 0 & H_2 \end{pmatrix}, \quad (149)$$

The usual method of doing the averaging is by considering the *partition function*:

$$\mathcal{Z} = \int \mathcal{D}\Phi e^{\Phi(H+qV)\Phi} = \int \mathcal{D}\Phi' e^{\Phi'(H_1+qV_1)\Phi'} \times \int \mathcal{D}\Phi'' e^{\Phi''(H_2+qV_2)\Phi'' + \Phi'(qV_B)\Phi'' + \Phi''(qV_A)\Phi'}. \quad (150)$$

After averaging over the short wavelength modes by performing the integral $\int \mathcal{D}\Phi''(\dots)$, a Φ' dependent expression will remain which is the generated interaction due to the short wavelength “mixing”. The result is a new *renormalized* perturbation potential, $q_{ren}V^{ren}$, defined by.

$$\mathcal{Z} = \int \mathcal{D}\Phi e^{\Phi(H+qV)\Phi} = \int \mathcal{D}\Phi' e^{\Phi'(H_1+q_{ren}V^{ren})\Phi'}. \quad (151)$$

We will see that for the single sink problem $q_{ren}V^{ren}$ has the same form as V_1 only the interaction strength gets renormalized $q \rightarrow q_{ren}$. The above mentioned procedure of performing the short-wavelength integral could be carried out but it was merely introduced to recapitulate the basics of renormalization group (RG) transformation. Instead, let us calculate $q_{ren}V^{ren}$ using GF-s and the diagrammatic technique introduced in Section III.

Single lines represent G^0 divided into long-, $G^{0'}$, and short-wavelength, $G^{0''}$, propagators, represented by single lines with a slash and single lines with double slash. Single lines with a wave represent the renormalized GF, $G^{ren} = (H_1 + q_{ren}V^{ren})^{-1}$. Crosses represents scatterings off qV and a cross in a circle represents $q_{ren}V^{ren}$ (see Figs. 15 and 16).

G^{ren} which is only defined for long wavelengths can be calculated using the original scattering potential, V . Scatterings of the long wavelength propagators can happen in two ways: *i*) a long wavelength propagator can scatter off V to a long wavelength propagator [Fig. 15(b)], and *ii*) a long wavelength propagator can scatter off V to short wavelength propagators and then scatter “back” to a long wavelength propagator [Fig. 15(c)], i.e., the scatterings of the long wavelength propagators are mediated by short wavelength propagators.

In Fig. 16(a), all the possible scatterings of the long wavelength propagators are represented. In Fig. 16(b) the scatterings are reordered introducing a new symbol, a cross in a circle that represents all the possible $G^{0''}$ mediated scatterings of $G^{0'}$ -s. Figure 16(c) is the reordering of Fig.16(b) to the similar form of a Dyson equation where one can identify \otimes as $q_{ren}V^{ren}$.

The sum in the formula of \otimes can be solved. Notice that this is exactly the same problem as that of Section III

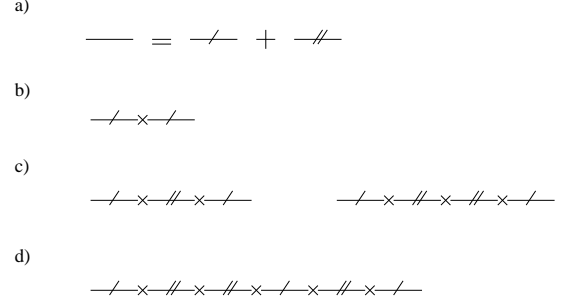


FIG. 15: Introduction of the short and long wavelength diagrams. a) Decomposition of the GF to short and long-wavelength modes. b) Simple scattering of the long-wavelength GF. c) Scatterings of the long-wavelength GF mediated by short-wavelength GF-s. d) A typical scattering with multiple scatterings between the long and short wavelength modes.

except that in that problem the intervening propagator between scatterings was G^0 while here $G^{0''}$. Therefore

$$\otimes = \frac{q}{1 + qG^{0''}(\mathbf{r} = \mathbf{0})} V_1 = q_{ren}V^{ren}, \quad (152)$$

where

$$G^{0''}(\mathbf{r} = \mathbf{0}) = \int_{1/l}^{1/a} \frac{d^d k}{k^2} \propto \begin{cases} l & \text{if } d = 1 \\ \ln l & \text{if } d = 2 \\ a^{2-d} & \text{if } 2 < d. \end{cases} \quad (153)$$

The dimensionality of q is $(length)^{d-2}$ [89] therefore after the fourth step of renormalization:

$$q \rightarrow \tilde{q} = q_{ren}l^{(2-d)}. \quad (154)$$

In one dimension, when $l \rightarrow \infty$,

$$\tilde{q} \propto \frac{q}{1 + ql} l \rightarrow const. \quad (155)$$

In two dimensions,

$$\tilde{q} \propto \frac{q}{1 + q \ln l} = \mathcal{O}\left(\frac{1}{\ln l}\right) \rightarrow 0. \quad (156)$$

For $d > 2$,

$$\tilde{q} \propto \frac{q}{1 + qa^{2-d}} l^{2-d} = \mathcal{O}(l^{2-d}) \rightarrow 0. \quad (157)$$

In conclusion, q is relevant in one dimension, marginally irrelevant in two dimensions, and irrelevant in higher dimensions.

For a single-link, there are two cases to be differentiated: *i*) When the separation of the two endpoints (λ) is much larger than the lengthscale over which the renormalization is carried out ($l \ll \lambda$). In this case, the vicinity of these endpoints can be considered as independent

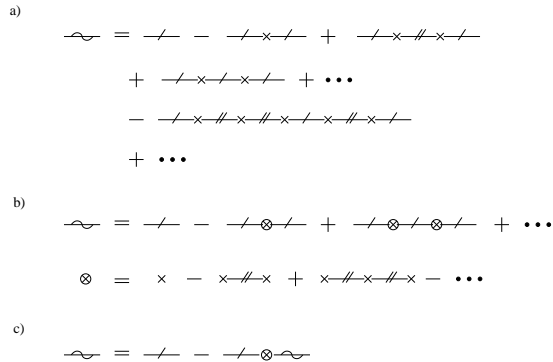


FIG. 16: Obtaining the renormalized GF for the single sink and link problem. a) The perturbation expansion of the renormalized GF, represented by a line with a wave. b) Introduction of the renormalized scattering operator, \otimes . c) The Dyson equation of the renormalized GF.

d -dimensional spaces for the short-wavelength GF to exist in, connected by a link at the origin with strength q . As in the case of a single sink, the renormalized interaction strength can be calculated using the diagrams of Fig. 16. As a result,

$$q_{ren} = \frac{q}{1 + 2qG^{0''}(\mathbf{r} = \mathbf{0})} \quad (158)$$

and the RG equation for the interaction strength, \tilde{q} , is the same as for the single-sink problem: (Eqs. (155, 156, 157)). ii) When $l \gg \lambda$, links and sinks get treated very differently: links can simply be ignored ($\tilde{q} = 0$) since the perturbation potential caused by a link has vanishing strength at these lengthscales while the effect of sinks can be still strong (see Eqs. (155, 156, 157)).

E. The renormalization of q including interactions between links and the scaling of the Green's function

We now combine the results for the RG flow of \tilde{p} in Eq. (145) with the results for \tilde{q} to describe the scaling of the Green's function on a small-world network. When \tilde{p} is small, we can use the single-link results for the scaling of \tilde{q} in Eqs. (155,156,157). When \tilde{p} becomes of order unity, however, these results will need to be modified.

Consider a network with p and q both much smaller than 1. If $\alpha < 2d$, then \tilde{p} is increasing under the flow and will eventually become of order unity. We will start by investigating this case. We restrict ourselves to the study of the case when $d < \alpha < 2d$, which is the most complicated one, for the sake of brevity. In the omitted case, $\alpha < d$, the derivation of the scaling properties can be obtained similarly using the results of the two previous sections.

We begin by studying the case when $d < \alpha < 2d$ and $d < 2$ (see Fig. 17). As long as both \tilde{p} and \tilde{q} are much smaller than unity, \tilde{q} obeys the naive scaling $\tilde{q} \propto l^{2-d}$. This naive scaling for \tilde{q} will break down when either \tilde{q}

becomes of order unity (due to multiple scattering off of a single link) or when \tilde{p} becomes of order unity (due to scattering off multiple links). So, we must determine whether it is \tilde{p} or \tilde{q} that becomes of order unity first. The link density, \tilde{p} becomes of order 1, from the naive scaling, at $l \sim (1/p)^{1/(2d-\alpha)}$, while \tilde{q} becomes of order unity, from the naive scaling, at $l \sim (1/q)^{1/(2-d)}$. So, if $(1/q)^{1/(2-d)} \ll (1/p)^{1/(2d-\alpha)}$ then \tilde{q} becomes of order unity first. That is, if $q \gg p^{(2-d)/(2d-\alpha)}$ then \tilde{q} becomes of order unity while \tilde{p} is still much smaller than unity. In this case, we can continue to use the single link results (155) for the RG flow of \tilde{q} and so \tilde{q} approaches a constant of order unity as the length scale continues to increase, while p still increases following Eq. (145). Thus, beyond this length scale, everything is set by the scaling of \tilde{p} and the original value of q becomes unimportant. Therefore, by dimensional analysis, using the scaling of $G(0)$, we find that $G(0) \sim p^{-(2-d)/(2d-\alpha)}$. On the other hand, if $q \ll p^{(2-d)/(2d-\alpha)}$, then \tilde{p} becomes of order unity while \tilde{q} is still much less than one. In this case, mean-field theory becomes accurate [90], and we find that $G(0) \sim (pq)^{(d-2)/(2+d-\alpha)}$. Thus,

$$\begin{aligned} q \gg p^{(2-d)/(2d-\alpha)} &\rightarrow G(0) \sim p^{-(2-d)/(2d-\alpha)} \quad (159) \\ q \ll p^{(2-d)/(2d-\alpha)} &\rightarrow G(0) \sim (pq)^{(d-2)/(2+d-\alpha)}. \end{aligned}$$

As a consistency check, note that the two expressions for $G(0)$ agree when $q \sim p^{(2-d)/(2d-\alpha)}$.

Next, consider the case that $d < \alpha < 2d$ and $d \geq 2$. For $d = 2$, we find that \tilde{q} is marginally irrelevant under the RG flow (156), decreasing inversely with the logarithm of the length scale. For $d < \alpha < 2d$, \tilde{p} will become of order unity at a scale $l \sim (1/p)^{1/(2d-\alpha)}$. The scale l is a power of p , hence the logarithm of the length scale is proportional to a logarithm of p . Thus, we can apply mean-field theory at this scale l with a $\tilde{q} \sim 1/\ln(1/p)$. Therefore, there are logarithmic corrections to mean-field theory for $d = 2$ and $G(0) \sim \ln(p/\ln p)$. In the case when $d < \alpha < 2d$ and $d > 2$, \tilde{q} is irrelevant and we can apply naive scaling until the scale $l \sim (1/p)^{1/(2d-\alpha)}$ at which point we can apply mean-field theory. Therefore, for $d > 2$, mean-field is always accurate in the limit of small p, q .

Finally, there is the case $\alpha = 2d$, when \tilde{p} is unchanging under the flow. For $d > 2$, \tilde{q} flows to zero, and then the effect of the links becomes negligible. However, for $d < 2$, \tilde{q} flows to a constant of order unity. Then we have a nontrivial fixed line of the RG flow with \tilde{p} arbitrary and \tilde{q} of order unity. This leads to a $G(0)$ which varies as an anomalous power of the system size, where the power depends continuously on the value of p .

Note that, when $\alpha > 2d$, \tilde{p} always flows to zero therefore the long-distance scaling of the GF becomes insensitive to the presence of the random links.

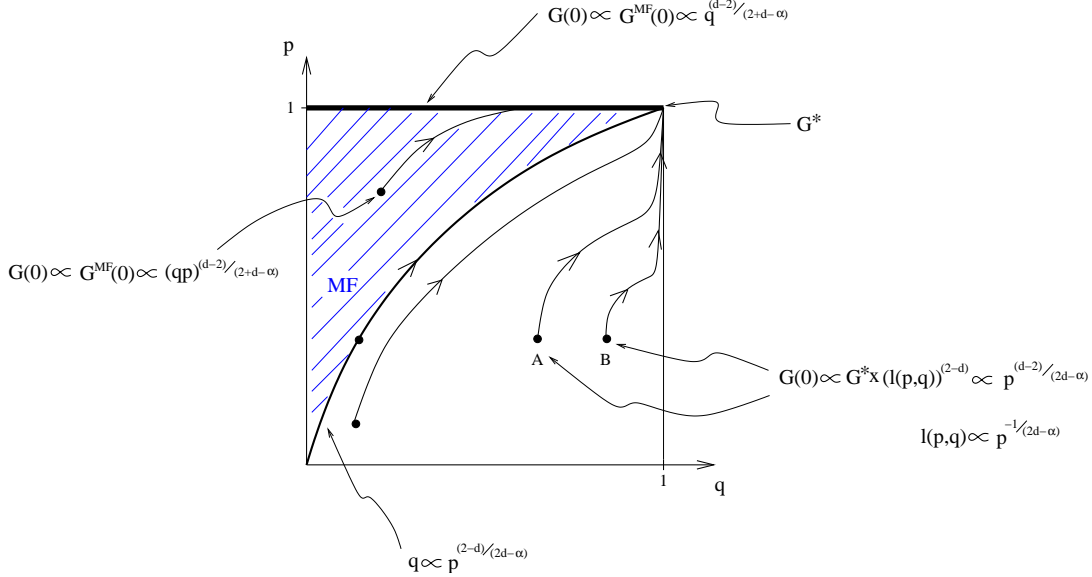


FIG. 17: The schematic representation of the RG flow when $d < 2$ and $d < \alpha < 2d$ for the quenched system. The parameter space is divided into two parts: i) where the behavior of the system is MF and ii) where the large-scale behavior is only determined by p . We also indicated the scaling of the GF in the two regimes. In part ii), consider two points in the phase space A and B with different q but the same p values: Renormalization transformed both systems to an identical one in the parameter space, where the GF is G^* . Furthermore, it took the same number of renormalization steps, l , to get to G^* from both points because l is only determined by p . As a consequence, considering that the GF can be well approximated by the free GF at small lengthscales (until \tilde{p} becomes of order unity): $G_A(0) \propto G_B(0) \propto G^* l^{(2-d)} \propto p^{\frac{2-d}{2d-\alpha}}$. In other words, $G(0)$ have the same scaling behavior in the two points.

V. APPLICATIONS AND NUMERICS

A. Calculating physical properties from the Green's function

In Section II and III, an impurity averaged perturbation expansion was set up to calculate the propagator of the diffusion operator for different configurations of the network by changing α , p , and q . Here we interpret the results for the GF in terms of the relevant observables of surface growth (Section IB) and random-walk processes (Section IA).

For EW processes, from Eq. (28),

$$[\langle w^2 \rangle] = \frac{1}{L^d} \sum_{i=1}^{L^d} [G_{ii}] = \frac{1}{L^d} \sum_{i=1}^{L^d} G(0) = G(0). \quad (160)$$

Similarly in the annealed case $[\langle w^2 \rangle]^{ann} = G^{ann}(0)$. Therefore, all the results derived for $G(0)$ can be translated in terms of the average width of the EW process, represented by the naming of the different phases of Figures 2 and 3

Though the perturbative calculations were done for $G(0)$, they can be repeated for $\hat{G}(0, \omega)$, defined in Eq. (18). The difference one has to consider is that, for the EW processes, the unperturbed GF is $G^0 = (\Delta^0)^{-1}$; for random-walks, it is $\hat{G}^0(\omega) = (\Delta^0 + \omega)^{-1}$. This substitution also results in a slight change in the Fourier space

calculations

$$G(k) = \frac{1}{k^2 + \Sigma(k)} \rightarrow \hat{G}(k, \omega) = \frac{1}{k^2 + \Sigma(k) + \omega}, \quad (161)$$

as can be seen in Fig. 27, where $\Sigma(k)$ is the self-energy generated by the random links as calculated in Sections II and III. In order to obtain the scaling properties of $\hat{G}(\mathbf{r}, \omega)$ and, specifically, of $\hat{G}(0, \omega)$, the approximations of Appendix B are used. As a general rule, in the case of $\hat{G}(k, \omega)$, the small- k divergence is cut off by the ω term in the denominator. Using the approximation of Eq. (19), the scaling of the expected number of returns can be related to $\hat{G}(0, \omega = 1/T)$ by

$$\begin{aligned} [F(T)] &\propto \frac{1}{L^d} \sum_{\mathbf{r}} [\hat{G}_{\mathbf{r}, \mathbf{r}}(\omega = 1/T)] + \frac{T}{L^d} \\ &= \frac{1}{L^d} \sum_{\mathbf{r}} \hat{G}(0, \omega = 1/T) + \frac{T}{L^d} \\ &= \hat{G}(0, \omega = 1/T) + \frac{T}{L^d}. \end{aligned} \quad (162)$$

Initially, we are only interested in the long-time behavior of the expected number of returns in the infinite system-size limit, therefore, $[F(T)] \propto \hat{G}(0, \omega = 1/T)$ in the thermodynamic limit. As it was done for the width of the EW process, the interpretation of the scaling of $\hat{G}(0, \omega = 1/T)$ as the scaling of the expected number

of returns is represented in the naming of the different phases of Figures 2 and 3. Later in this section, we will also see how the finite size of the system changes the behavior of $F(T)$.

B. Numerical approach

Numerical results were obtained in one-dimension ($N = L$). In order to check the analytic predictions of Section III, we numerically calculated different physical properties of the processes introduced in Section I. For the quenched networks, numerical results were obtained by: (i) generating a large number of realizations (from 100 to 1000) of PL-SW networks, then (ii) generating the diffusion operator, Eq. (4), on each realization, then (iii) using exact numerical diagonalization [79] to obtain the eigensystem of the diffusion operator on each realization, then (iv) using the spectral decomposition of the different physical quantities, Eqs. (29) and (16), to obtain their value for each realization; then (v) averaging these quantities over a large number of realizations of the networks.

For the annealed networks, we numerically integrated the corresponding time-discretized stochastic EW process in a dynamically annealed network: at every time step the *random links*, with density p , are reassigned. The EW equation was numerically integrated using the most basic time-discretization scheme

$$\begin{aligned} h_i(t + \Delta t) &= h_i(t) + \Delta t [h_{i+1}(t) + h_{i-1}(t) - 2h_i(t)] \\ &+ \Delta t q A_{i,r(i)}(t) [h_{r(i)}(t) - h_i(t)] \\ &+ \eta_i(t) \sqrt{2\Delta t}, \end{aligned} \quad (163)$$

where unit lattice spacing for the underlying regular lattice is assumed, $\eta_i(t)$ -s are independent and identically distributed random variables for all i and t with Gaussian distribution of zero mean and unit variance, and $r(i)$ is the random neighbor of node i at time t . In this annealed construction, at every time step, each node has a random neighbor with probability p ; $A_{i,r(i)}=1$ if node i has a random neighbor, $A_{i,r(i)}=0$ otherwise. At every time step the random links are independently reassigned, a new PL-SW-network configuration is generated. For the time-discretization scheme to be convergent for the EW process on any *fixed* network, one can show that

$$|\Delta t \lambda_{\max} - 1| < 1, \quad (164)$$

i.e., $\Delta t < 2/\lambda_{\max}$ is required, where λ_{\max} is the largest eigenvalue of the network Laplacian. While for the annealed network, where the network changes at every time step, we do not have a similar rigorous requirement, as a guiding estimate, one can consider the largest eigenvalue of the *average* (annealed) Laplacian. For example, for $\alpha < 1$ PL-SW networks, using our results for the annealed random Laplacian [Eq. (39)] (embedded in dis-

crete lattices), one has

$$\begin{aligned} \lambda_{\max}^{\text{ann}} &\sim \max_k \{2[1 - \cos(k)] + [\Delta^{rnd}](k)\} \\ &= \max_k \{2[1 - \cos(k)] + Cqp\} = 4 + Cqp, \end{aligned} \quad (165)$$

where C is a constant which does *not* depend on p , q , and the system size N . The resulting time-discretization scheme then requires

$$\Delta t \lesssim \frac{2}{4 + Cpq}. \quad (166)$$

Similarly, for $1 < \alpha < 3$, one finds

$$\Delta t \lesssim \frac{2}{4 + Cpq4^{\alpha-1}}. \quad (167)$$

The important consequence of the above order-of-magnitude estimates for the time discretization is that for *annealed* plain or PL-SW networks, Δt does not depend on the system size. Thus, if a sufficiently small Δt is tested and confirmed to lead to a converging scheme for a small system size, it will do so for all system sizes [91]. In our numerical integrations, we used $\Delta t = 0.10$, which turned out to be sufficient to achieve numerical convergence for the values $q = 1$ and $p \leq 1$ considered here.

C. Roughness scaling on plain SW networks

In Section III, for plain SW networks ($\alpha = 0$), it was shown that the MF approximation is valid in the high density of weak links limit ($q \rightarrow 0$) and $[\langle w^2 \rangle] \propto q^{-1/2}$, but breaks down when the number of random links is small ($p \rightarrow 0$). In the later case, the self-consistent perturbation expansion yielded $[\langle w^2 \rangle] \propto p^{-1}$. In Fig. 18, we compared our analytic predictions to numerical results and found a good agreement between the numerics and the analytics for an intermediate interval of q and p . For small values finite-size effects are observed, addressed in Section V F.

D. Roughness scaling in transient/smooth phase II and in recurrent/rough phases for annealed and quenched networks

In Fig. 19, the different scaling behavior of the annealed and quenched system is shown in transient/smooth phase II ($\alpha=1.4$). The quenched results were obtained by exact numerical diagonalization techniques, and the annealed results were produced by integrating the stochastic EW process in a dynamically annealed network, as described above. As can be seen in Fig. 19, the numerical results and the annealed analytic prediction are in good agreement.

For the annealed case, Fig. 20 shows the system-size dependence of the width (or $G(0)$) in transient/smooth phase II ($\alpha=1.4$) and in recurrent/rough phase II

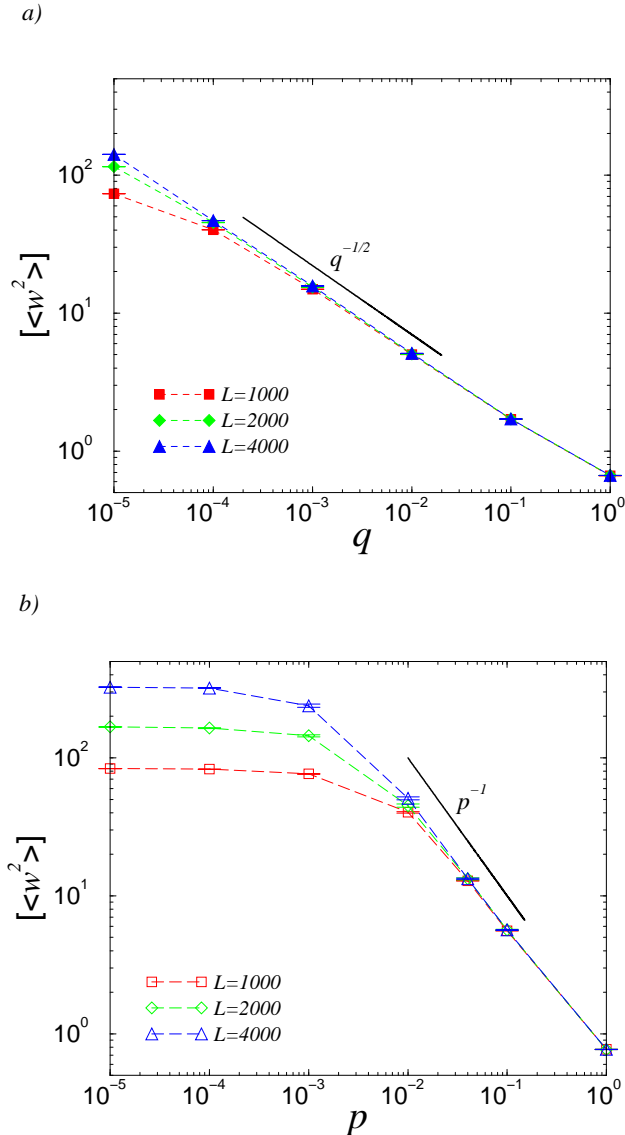


FIG. 18: Disorder averaged width obtained by exact numerical diagonalization of the diffusion operator (a) changing the strength of the long-range links while keeping their density fixed ($p = 1$); and (b) changing the density of the long-range links while keeping the strength constant ($q = 1$) for system sizes indicated in the figure. The two slopes indicate the analytic predictions in the two cases. Note that the MF argument would predict the same behavior for both cases.

($\alpha=2.5$). The agreement between the analytic predictions (summarized in Fig. 2) and the simulation of the EW process in an annealed random network is good in the asymptotic large system-size limit.

Figure 21 shows numerical results (from numerical diagonalization) for both rough phases in quenched networks. For the quenched case, the recurrent/rough phase II is somewhat “degenerate” in that it collapses onto a single point, $\alpha=2$ (Fig. 2). Here, the asymptotic analytic results indicated that the exponent of the divergence depends continuously on p , $G(0) \sim L^{\gamma(p)-2}$

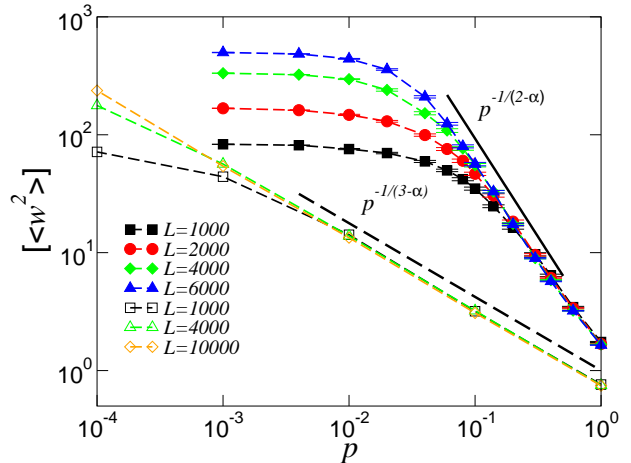


FIG. 19: Numerically obtained finite-size propagators $G(0)$ vs. p for $\alpha=1.4$, $q=1$ (transient/smooth phase II) for various system sizes. Solid symbols represent data obtained by exact numerical diagonalization averaged over 100 realizations for the quenched network. The solid straight line represents the slope obtained from the perturbative analytic calculations in the $L \rightarrow \infty$ limit. Open symbols correspond to the steady-state averaged propagator on the annealed network with the straight dashed line being the analytic result for the annealed system in the $L \rightarrow \infty$ limit.

[Eq. (93)]. Although the self-consistent formula predicts this feature *qualitatively* (not shown on the plot for the sake of clarity), the actual exponent appears to be strongly affected by higher-order corrections. In the recurrent/rough phase I, the width diverges as $G(0) \sim L$, just as in a network without long-range links.

E. Short- and long-time behavior of the expected number of returns of a random walker on PL-SW networks

In experimental and numerical setups, it is important to understand the behavior of the observed quantities for finite times and finite system sizes in order to interpret the results. Because of finite system sizes, one can observe different crossovers in the behavior of the expected number of returns of a random walker. One of the crossover times, T_{\times} , can be predicted by studying the integral representation of $\hat{G}(0, \omega = 1/T)$ in Eq. (162): determining whether, at timescale T , the behavior of the integral is dictated by the k^2 term or by $\Sigma(k)$, the self-energy generated by the random links. The other crossover happens at times, $T_{\times\times}$, when $T_{\times\times}/L^d \approx \hat{G}(0, \omega = 1/T_{\times\times})$. For $T \gg T_{\times\times}$, the scaling of $F(T)$ is dominated by finite-size effects.

As an example, let us have a closer look at transient phase II. Before $T_{\times} \propto p^{\frac{-2}{2-\alpha}}$, the expected number of returns scales as that of a regular one-dimensional walker; for later times, typically, the walker escapes from the vicinity of the origin through some long-range link;

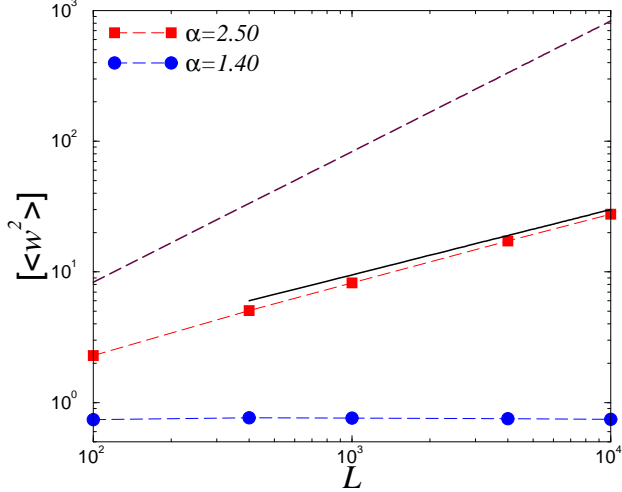


FIG. 20: System-size dependence of the width obtained by numerically integrating the EW process on annealed PL-SW networks [Eq. (163)] (for $q=1$ and $p=1$) at a representative point in the transient/smooth phase II ($\alpha=1.4$) and in the recurrent/rough phase II ($\alpha=2.5$). The solid line corresponds to the analytically-predicted asymptotic scaling in the recurrent/rough phase II, $G(0) \sim L^{\alpha-2}$. The dashed line indicates the exact scaling behavior in a network with no long-range links in one dimension, $G(0) \sim L$, as a reference.

though, after $T_{\times\times} \propto Lp^{\frac{1}{2-\alpha}}$, the walker starts to return “from the perimeter” of the network due to the finite size of the system.

In Fig. 22(a), we show the sketch of the scaling predictions for $F(T)$ as discussed above. In Fig. 22(b), we show the disorder-averaged $F(T)$, obtained by employing Eq. (16) with the eigenvalues from exact numerical diagonalization, for each realization of the network, and averaging over 100 realizations. The two plots compare very well.

F. Finite-size behavior and scaling functions

Up to this point, in the analytic forms, we mostly considered the infinite system-size behavior of the width, although it is clear from the plots, Figs. 18 and 19, that in the limit of weak long-range interactions the divergence of the width is cut off by system size effects. This observation is plausible since in the case $p \rightarrow 0$ (or $q \rightarrow 0$ obviously) the width should not have a stronger divergence than the pure (in this case one-dimensional) lattice. Therefore, one can conclude that for $p = 0$ (the limit of a regular one-dimensional network) $[\langle w^2 \rangle] \sim L$, while for $p \neq 0$, in the infinite system-size limit, it approaches a constant, $[\langle w^2 \rangle] \simeq 1/\sqrt{\Sigma} = \xi$ [see Fig. 23(a)]. Thus, the finite-size behavior of the average width can be expressed as

$$[\langle w^2 \rangle] = Lf(\xi/L), \quad (168)$$

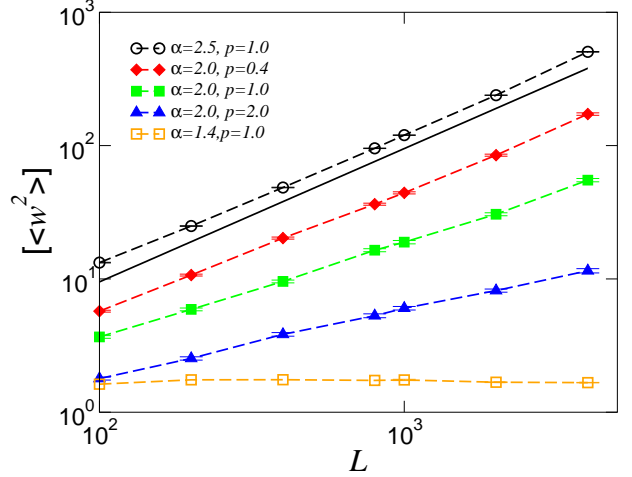


FIG. 21: Comparison of system-size dependence of the width calculated by exact numerical diagonalization (all data for $q=1$) for representative α -s from different phases of the quenched network as predicted in Fig. 3. Data in the recurrent/rough phase I (\circ symbols) indicate the linear scaling with L (data is shifted up for clarity). Filled symbols represent the scaling behavior in the recurrent/rough phase II ($\alpha=2$) for various values of p , indicating the p -dependence of the exponent. The solid line represents the linear system-size dependence to guide the eye. Data in the transient/smooth phase II (\square symbols), indicating a finite $G(0)$ in the $L \rightarrow \infty$ limit, are also shown for comparison.

where $f(x)$ is a scaling function such that

$$f(x) \sim \begin{cases} x & \text{if } x \ll 1 \\ \text{const.} & \text{if } x \gg 1. \end{cases} \quad (169)$$

For the hard SW network, $\Sigma = q + \dots$ hence $\xi = 1/\sqrt{q}$. The scaled numerical data, $[\langle w^2 \rangle]/L$ vs $q^{-1/2}/L$ in Fig. 23(b), shows good collapse, as suggested by Eq. (168).

In Fig. 24, for quenched plain SW networks, a similar finite-size correction can be observed. From the perturbative calculations $\Sigma \propto p^2$ but the constant factor and higher-order terms were undetermined. In conclusion, $\xi \propto p^{-1}$. Using this knowledge and doing the same scaled plot as for the hard network, a good data collapse is observed, though due to our lack of knowledge about the accurate behavior of ξ the scaling function is not as precise as in the hard case.

Strictly speaking, power-law networks do not have a correlation length like plain SW networks ($\alpha = 0$). Still, something can be said about the finite-size behavior, as observed in Fig. 19. In the general case, there are two competing terms determining the large scale behavior of the Green’s function, - the diffusion through the regular links, Δ , and through the random ones, Δ^{rnd} . At small length scales, the number of the random links is small, their contribution to the ensemble average is negligible, and the behavior is close to that of a d -dimensional unperturbed system. The effect of the random interac-

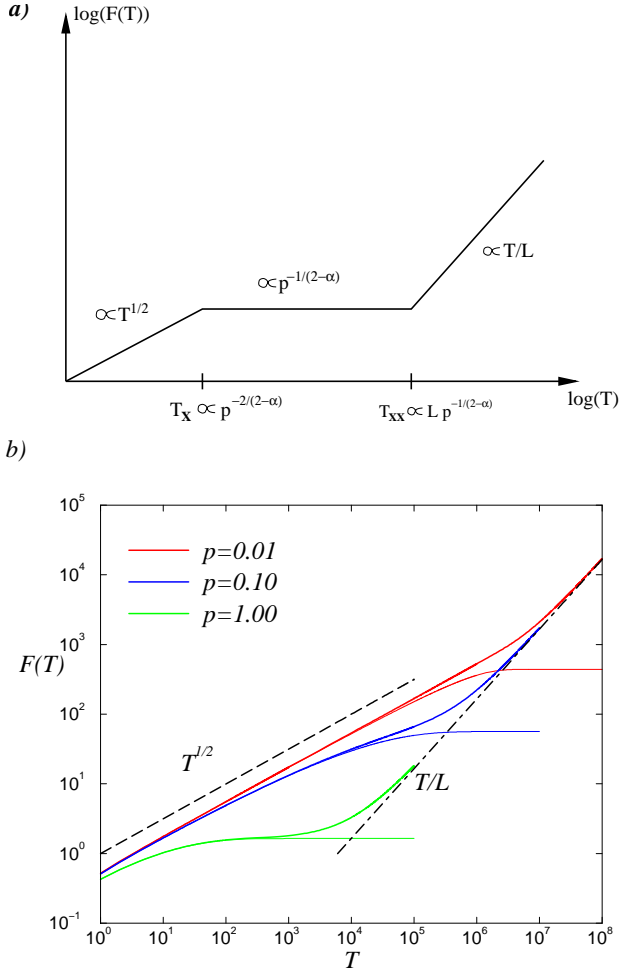


FIG. 22: (a) The analytic prediction for the expected number of returns and (b) its numerical verification (fat lines) in transient phase II on a quenched PL-SW network with $\alpha = 1.4$, $L = 6000$, and $q = 1$. Thin lines represent numerical results obtained by excluding the effect of the uniform mode in Eq. (16) responsible for the “finite-size” behavior for large T values.

tions takes over when the self-energy generated by these random links start to dominate the infrared behavior of $G(k)$, which is when $k_\times^2 \approx \Sigma(k_\times)$. Having these different regimes and crossovers, one can construct a scaling function of $G(0)$ for finite systems similar to the one of plain SW networks:

$$[\langle w^2 \rangle] = G(0) = Lf(L_\times/L) \quad (170)$$

where $L_\times = k_\times^{-1} \propto p^{\frac{-1}{2-\alpha}}$ in transient/smooth phase II. The collapse of the scaled numerical data in Fig. 25 supports the validity of the above construction, though slight deviation can be observed from the predicted straight line for large system sizes.

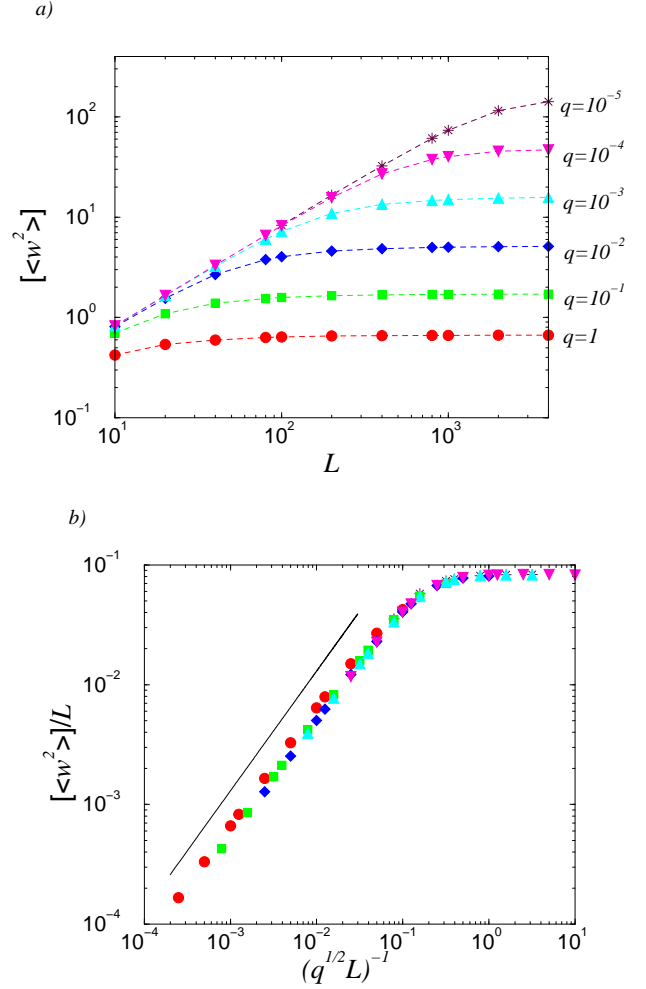


FIG. 23: (a) The system-size dependence of the width for different random connection strengths (q -s) on hard SW networks. (b) The data of (a) collapsed to a single curve approximating Σ to first order in q and rescaling the axes according to Eq. (168). Solid-line segments correspond to the asymptotic small- x behavior of the scaling function $f(x)$ given in Eq. (169).

G. Disorder-averaged two-point function

Finally, let us investigate the spatial behavior of the disorder-averaged GF, $G(l)$ for quenched plain SW networks. From Eq. (77), $\Sigma(k) \propto p^2$, i.e. the GF is massive. In this case, from Eq. (D3),

$$[G(l)] \simeq \frac{1}{2\sqrt{\Sigma}} e^{-\sqrt{\Sigma}l}, \quad (171)$$

In Fig. 26 we compared the above analytic result with ones from exact numerical diagonalization and found good agreement up to finite-size effects at large distances.

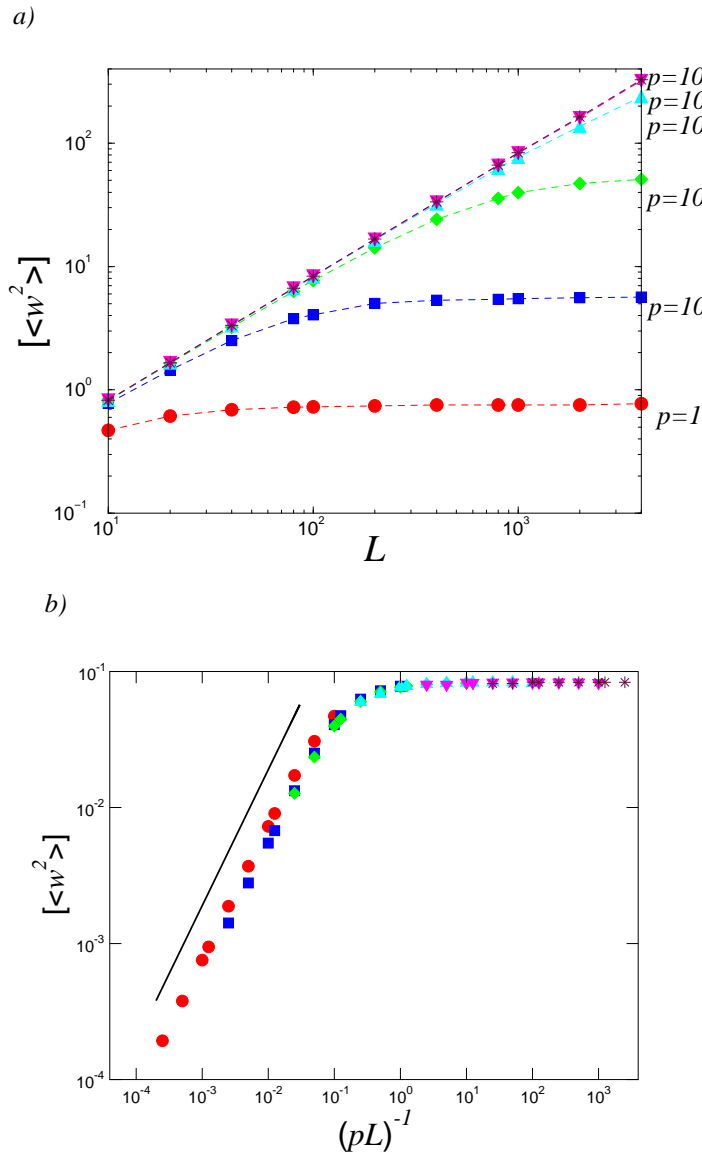


FIG. 24: (a) Width as a function of the system size with different crossovers for different p -s for quenched plain SW networks. (b) Collapse of the same data to yield the scaling function Eq. (169). The solid-line segment correspond to the asymptotic small- x behavior of the scaling function $f(x)$ given in Eq. (169).

VI. SUMMARY

The addition of random long-range links to a regular d -dimensional network, producing a SW network, leads in many cases to a crossover to mean-field-like behavior [38], effectively becoming equivalent to averaging over the long-range links in an annealed fashion. Here, we investigated diffusion processes on distance-dependent SW networks, where it is *not* the case (in low dimensions), and the contrast between the quenched and annealed systems is strong. The results are summarized in the phase diagrams of Figs. 2 and 3, with dramatically different be-

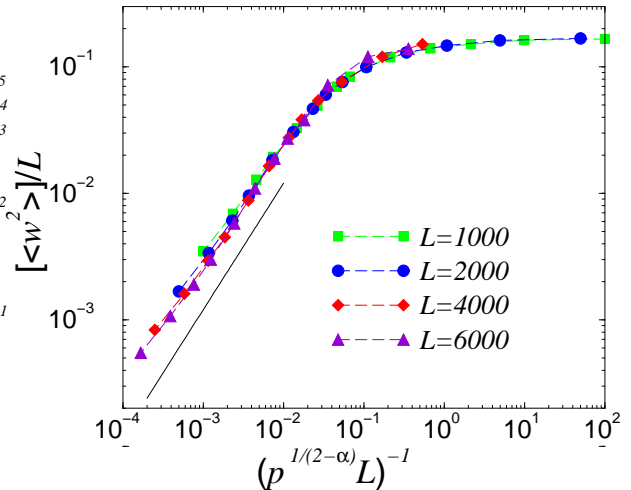


FIG. 25: The scaling function Eq. (170) for quenched PL-SW networks with $\alpha = 1.4$ obtained by exact numerical diagonalization of the diffusion matrix. The straight line represents the slope predicted by the finite-size scaling argument.

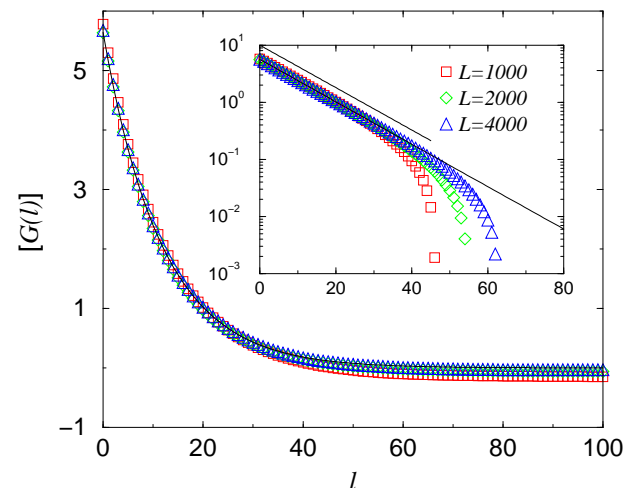


FIG. 26: Disorder-averaged two-point function as a function of the separation l in simple SW networks for $p = 0.10$ and three system sizes. The solid line corresponds to the exponential decay given by Eq. (171). The inset shows the same data in linear-log plot.

havior in the quenched and annealed case. The results for the quenched network were obtained by self-consistent perturbation theory. Although the formalism was set up for the propagator of the diffusion operator, it can be applied to other processes where the mean-field behavior is violated or, if the mean-field theory holds, to obtain higher-order corrections to it. We also demonstrated the validity of the asymptotic theoretical results by providing extensive numerical data based on the spectral decomposition of the coupling matrix and numerical integration of the stochastic EW process.

Acknowledgments

Discussions with H. Guclu, Z. Toroczka, M.A. Novotny, L.A. Braunstein, Z. Rácz, G. Györgyi, and T. Antal are gratefully acknowledged. This research was supported in part by NSF Grant No. DMR-0426488, the Research Corporation, and RPI's Seed Grant. M.B.H. was supported by the U.S. DOE at LANL under Contract No. DE-AC52-06NA25396. B.K. was partially supported by the EU under contract 001907 (DELIS).

APPENDIX A: THE FOURIER TRANSFORM OF THE DIFFUSION OPERATOR

In a general case, the real space behavior of the averaged diffusion operator (or self-energy) is

$$[\Delta^{rnd}]_{\mathbf{r},\mathbf{r}'} = \begin{cases} p & \text{if } \mathbf{r} = \mathbf{r}' \\ \frac{-p}{\mathcal{N}} \frac{1}{|\mathbf{r}-\mathbf{r}'|^\alpha} & \text{if } \mathbf{r} \neq \mathbf{r}' \end{cases} \quad (\text{A1})$$

Multiplying it with a Fourier mode, $e^{i\mathbf{k}\mathbf{r}'}$,

$$\begin{aligned} \sum_{\mathbf{r}'} [\Delta^{rnd}]_{\mathbf{r},\mathbf{r}'} e^{i\mathbf{k}\mathbf{r}'} &= p \frac{\mathcal{N}}{\mathcal{N}} e^{i\mathbf{k}\mathbf{r}} - \frac{p}{\mathcal{N}} \sum_{\mathbf{r}' \neq \mathbf{r}} e^{i\mathbf{k}\mathbf{r}'} \frac{1}{|\mathbf{r}-\mathbf{r}'|^\alpha} \\ &= \frac{p}{\mathcal{N}} e^{i\mathbf{k}\mathbf{r}} \sum_{\mathbf{r}' \neq \mathbf{r}} \frac{1}{|\mathbf{r}-\mathbf{r}'|^\alpha} (1 - e^{i\mathbf{k}(\mathbf{r}'-\mathbf{r})}) \\ &= \frac{p}{\mathcal{N}} e^{i\mathbf{k}\mathbf{r}} \sum_{\mathbf{r}'' \neq 0} \frac{1}{|\mathbf{r}''|^\alpha} (1 - e^{i\mathbf{k}\mathbf{r}''}). \end{aligned} \quad (\text{A2})$$

The Fourier vectors are eigenvectors of the matrix with eigenvalues

$$[\Delta^{rnd}](\mathbf{k}) = \frac{p}{\mathcal{N}} \sum_{\mathbf{r}'' \neq 0} \frac{(e^{i\mathbf{k}\mathbf{r}''} - 1)}{|\mathbf{r}''|^\alpha}. \quad (\text{A3})$$

or, in the continuum limit,

$$[\Delta^{rnd}](\mathbf{k}) = \frac{p}{\mathcal{N}} \int d^d r \frac{e^{i\mathbf{k}\mathbf{r}} - 1}{r^\alpha}. \quad (\text{A4})$$

Next, the scaling properties of $[\Delta^{rnd}](\mathbf{k})$ are calculated, when $a \ll 1/k \ll L$. For this reason \mathcal{N} is also approximated by its integral-form limit

$$\mathcal{N} = \sum_{i=1}^{L^d} \frac{1}{r^\alpha} \propto \int_a^L r^{d-1} dr \frac{1}{r^\alpha} \propto \begin{cases} L^{d-\alpha} & \text{if } \alpha < d \\ \ln(L/a) & \text{if } \alpha = d \\ a^{d-\alpha} & \text{if } d < \alpha \end{cases} \quad (\text{A5})$$

The approximations of the formulae below follow those of Appendix C, Eqs. (C3) and (C9):

$$\begin{aligned} \int_a^L d^d r \frac{1 - e^{i\mathbf{k}\mathbf{r}}}{r^\alpha} &= \int_a^L \frac{1 - \cos(kx)}{x^\alpha} dx \\ &\propto k^2 \int_a^{1/k} \frac{dx x^2}{x^\alpha} + \int_{1/k}^L \frac{dx}{x^\alpha} \\ &\propto \begin{cases} L^{1-\alpha} & \text{if } \alpha < 1 \\ k^{\alpha-1} & \text{if } 1 < \alpha < 3 \\ k^2 a^{3-\alpha} & \text{if } 3 < \alpha \end{cases} \end{aligned} \quad (\text{A6})$$

In higher dimensions,

$$\begin{aligned} \int_a^L d^d r \frac{1 - e^{i\mathbf{k}\mathbf{r}}}{r^\alpha} &= \int_a^L dr r^{d-1} \int d\Omega \frac{1 - e^{i\mathbf{k}\mathbf{r} \cos \theta}}{r^\alpha} \\ &\propto k^2 \int_a^{1/k} \frac{dr r^{2d-1}}{r^\alpha} + \int_{1/k}^L \frac{dr r^{d-1}}{r^\alpha} \\ &\propto \begin{cases} L^{d-\alpha} & \text{if } \alpha < d \\ \ln(kL) & \text{if } \alpha = d \\ k^{\alpha-d} & \text{if } d < \alpha < d+2 \\ k^2 |\ln(ka)| & \text{if } \alpha = d+2 \\ k^2 a^{d+2-\alpha} + \dots & \text{if } d+2 < \alpha \end{cases} \end{aligned} \quad (\text{A7})$$

Therefore, at leading order, assuming $a = 1$ without loss of generality,

$$[\Delta^{rnd}](\mathbf{k}) \propto \begin{cases} p & \text{if } \alpha < d \\ p \left(1 + \frac{\ln k}{\ln L}\right) & \text{if } \alpha = d \\ pk^{\alpha-d} & \text{if } d < \alpha < d+2 \\ pk^2 |\ln k| & \text{if } \alpha = d+2 \\ pk^2 + \dots & \text{if } d+2 < \alpha \end{cases} \quad (\text{A8})$$

In Subsection III F, the behavior of the Fourier transform of $\Sigma(\mathbf{r}) = \frac{s}{n r^4 \ln^\mu(r/a)}$ is needed in two dimensions when $0 > \mu > 1$:

$$\begin{aligned} \Sigma(k) &= \frac{s}{n} \int_a^L \frac{(J_0(kr) - 1)}{r^4 \ln^\mu(r/a)} r dr \\ &\propto \frac{s}{n} k^2 \int_a^{1/k} \frac{1}{r \ln^\mu(r/a)} dr + \dots \\ &\propto \frac{sc_1(\mu)}{n} k^2 \ln^{1-\mu}(ka) + \mathcal{O}\left(\frac{k^2}{\ln^\mu(ka)}\right), \end{aligned} \quad (\text{A9})$$

where $c_1(\mu)$ is a constant, the result of the Fourier transformation.

For the present purposes of this work in most cases the scaling behavior of $[\Delta^{rnd}](k)$ is sufficient to know. For more accurate calculations, one has to cope with the divergences of the integrals at their limits (for example, by introducing counterterms to the integrands) so as to

obtain the constants in the formulae. Since it is necessary in Subsection III E, let us calculate $\Sigma(k)$ (or equivalently $[\Delta^{rnd}](k)$) with more scrutiny in one dimension when $2 < \alpha < 3$:

$$\begin{aligned}\Sigma(k) &= 2\frac{s}{n}\Re \int_a^L \frac{1 - e^{ikr}}{r^\gamma} dr = 2\frac{s}{n}\Re i \int_a^L \frac{1 - e^{-kr}}{(ir)^\gamma} dr \\ &= 2\frac{s}{n}\sin\left(\frac{\pi}{2}\gamma\right) \int_0^\infty \frac{1 - e^{-kr}}{r^\gamma} dr \\ &= 2\frac{s}{n}k^{\gamma-1}\sin\left(\frac{\pi}{2}\gamma\right)\Gamma(1-\gamma)\end{aligned}\quad (\text{A10})$$

where \Re is the real part of a complex function. In the above steps, we transformed the complex contour integral from the real axis to the imaginary one between ia and iL , and then moved these limits to 0 and ∞ since the integrand was convergent at these limits and the main contribution of the integral comes from k values $\propto 1/r$ while $a \ll r \ll L$.

APPENDIX B: THE SCALING PROPERTIES OF $G(0)$ AND $G(0, \omega = 1/T)$

Most of the results of this paper are derived for $G(r = 0)$, or $G(0)$ for short, and $G(r = 0, \omega)$. Here, their scaling properties are obtained for general $\Sigma(k)$ -s when

$$G(k) = \frac{1}{k^2 + \Sigma(k)} \quad (\text{B1})$$

and similarly

$$G(k, \omega) = \frac{1}{k^2 + \Sigma(k) + \omega} \quad (\text{B2})$$

First, let us investigate $G(0)$

$$\begin{aligned}G(0) &= \int \frac{d^d k}{(2\pi)^d} \frac{1}{k^2 + \Sigma(k)} \\ &= \frac{S_{d-1}}{(2\pi)^d} \int_{1/L}^{1/a} \frac{k^{d-1} dk}{k^2 + \Sigma(k)}\end{aligned}\quad (\text{B3})$$

Since, in the present work, our interest is only in the scaling properties of $G(0)$, the following approximations are made: for different k values $G(k)$ is dominated by different terms in the denominator of Eq. (B1), as it is demonstrated in Fig. 27 for the specific case when $\Sigma(k) = sk^{\alpha-d}$. The crossover between the different regimes is determined by k_\times defined by $k_\times^2 = \Sigma(k_\times)$. From now on we assume that

$$\frac{\Sigma(k)}{k^2} \xrightarrow{k \rightarrow 0} 0. \quad (\text{B4})$$

As can be seen in Fig. 27,

$$\frac{1}{k^2 + \Sigma(k)} \approx \begin{cases} \frac{1}{\Sigma(k)} & \text{if } k \ll k_\times \\ \frac{1}{k^2} & \text{if } k_\times \ll k. \end{cases} \quad (\text{B5})$$

Therefore,

$$G(0) \propto \int_{1/L}^{k_\times} \frac{k^{d-1} dk}{\Sigma(k)} + \int_{k_\times}^{1/a} \frac{k^{d-1} dk}{k^2}. \quad (\text{B6})$$

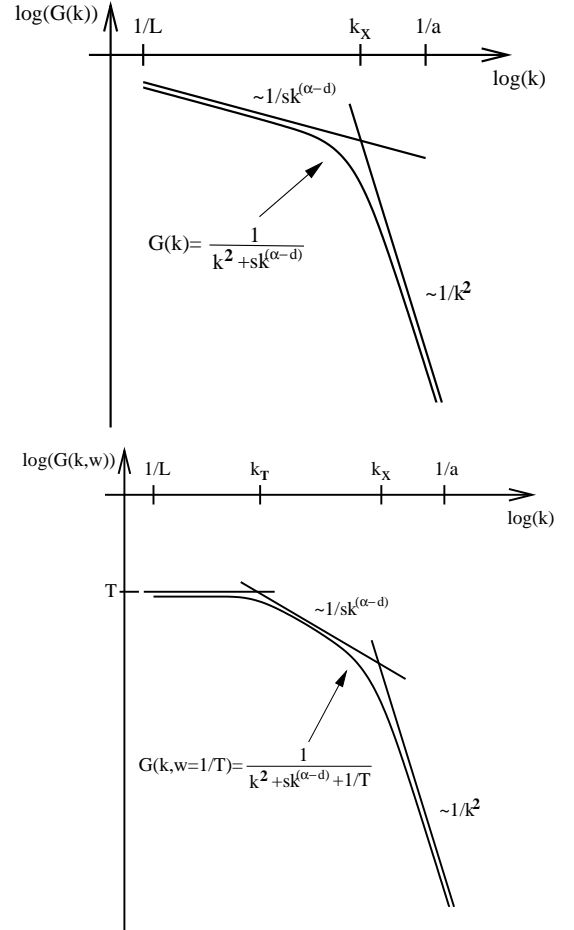


FIG. 27: A sketch of the approximations used in Eq.-s (B5) and (B11) to obtain the scaling of $G(0)$ and $G(0, \omega = 1/T)$ for the specific case when $\Sigma(k) = sk^{\alpha-d}$.

Next, $G(0)$ will be calculated for specific $\Sigma(k)$ as appear in the paper:

(i) If $\Sigma(k) = s$, $k_\times = \sqrt{s}$ and

$$\begin{aligned}G(0) &\propto \int_{1/L}^{k_\times} \frac{k^{d-1} dk}{s} + \int_{k_\times}^{1/a} \frac{k^{d-1} dk}{k^2} \\ &= \begin{cases} s^{-1/2} & \text{if } d = 1 \\ \ln(sa^2) & \text{if } d = 2 \\ a^{2-d} & \text{if } d \geq 3. \end{cases}\end{aligned}\quad (\text{B7})$$

(ii) $\Sigma(k) = sk^{\alpha-d}$ where $d < \alpha < d+2$ [92], $k_\times = s^{\frac{1}{2+d-\alpha}}$

and

$$\begin{aligned}
G(0) &\propto \int_{1/L}^{k_\times} \frac{k^{d-1} dk}{s k^{\alpha-d}} + \int_{k_\times}^{1/a} \frac{k^{d-1} dk}{k^2} \\
&= \frac{1}{s} [k^{2d-\alpha}]_{1/L}^{k_\times} + [k^{d-2}]_{k_\times}^{1/a} \\
&= \begin{cases} s^{\frac{-1}{3-\alpha}} & \text{if } d=1 \text{ and } \alpha < 2 \\ s^{-1} \ln(sL) & \text{if } d=1 \text{ and } \alpha = 2 \\ \frac{1}{s} L^{\alpha-2} & \text{if } d=1 \text{ and } 2 < \alpha \\ \ln(sa^{\alpha-4}) & \text{if } d=2 \\ a^{2-d} & \text{if } d \geq 3. \end{cases}
\end{aligned} \tag{B8}$$

(iii) $\Sigma(k) = sk^2 |\ln(ka)|$, $k_\times = \frac{1}{a} e^{1/s}$ and

$$\begin{aligned}
G(0) &\propto \int_{1/L}^{k_\times} \frac{k^{d-1} dk}{s k^2 |\ln(ka)|} + \int_{k_\times}^{1/a} \frac{k^{d-1} dk}{k^2} \\
&\propto \frac{1}{s} [(d-2)^{-1} k^{d-2} |\ln(ka)|^{-1}]_{1/L}^{k_\times} + [k^{d-2}]_{k_\times}^{1/a} \\
&\propto \begin{cases} \frac{L}{s \ln L} & \text{if } d=1 \\ \frac{1}{s} \ln \ln L & \text{if } d=2 \\ a^{2-d} & \text{if } d \geq 3. \end{cases}
\end{aligned} \tag{B9}$$

(iv) $\Sigma(k) = sk^2$, $\Sigma(k)$ is negligible to the k^2 term in the integral and the calculation is straightforward

$$G(0) \propto \begin{cases} L & \text{if } d=1 \\ \ln(L/a) & \text{if } d=2 \\ a^{2-d} & \text{if } d \geq 3. \end{cases} \tag{B10}$$

Note that a similar approximation can be done as above for $G(0, \omega = 1/T)$ (see Fig. 27). Introducing k_T , defined as $1/T = \Sigma(k_T)$,

$$\frac{1}{k^2 + \Sigma(k) + 1/T} \approx \begin{cases} T & \text{if } k \ll k_T \\ \frac{1}{\Sigma(k)} & \text{if } k_T \ll k \ll k_\times \\ \frac{1}{k^2} & \text{if } k_\times \ll k. \end{cases} \tag{B11}$$

Though, one must be careful because, for some $\Sigma(k)$, the definition of k_T cannot be satisfied for any k -s (while $1/L < k < 1/a$): for example, if $\Sigma(k) = s$ and T is

large. This tells us that the $1/T$ term is irrelevant in the integrand while calculating the scaling properties of $G(0, \omega = 1/T)$, the low k behavior is not affected by $1/T$ (for calculational purposes one may interpret it as $k_T = 1/L$). Another case one must be careful with, is when $k_T > k_\times$: in this case $\Sigma(k)$ becomes irrelevant in the determination of the integral since this case corresponds to the scenario that $1/T$ cuts off the low k behavior even before $\Sigma(k)$ would have contributed to the integral at all (see Fig. 27). Keeping these in mind the calculation of the scaling of $G(0, \omega)$ is straightforward.

APPENDIX C: THE SCALING PROPERTIES OF $(G(0) - G(r))$

Since $(G(0) - G(r))$ appears frequently in the calculations, its long-distance properties are calculated and summarized in this section.

$$\begin{aligned}
(G(\mathbf{0}) - G(\mathbf{r})) &= \int \frac{1 - e^{i\mathbf{k}\cdot\mathbf{r}}}{k^2 + \Sigma(k)} \frac{d^d k}{(2\pi)^d} \\
&= \int_{1/L}^{1/a} \frac{dk k^{d-1}}{(2\pi)^d} \int d\Omega \frac{1 - e^{i\mathbf{k}\cdot\mathbf{r} \cos \theta}}{k^2 + \Sigma(k)}.
\end{aligned} \tag{C1}$$

In one dimension,

$$(G(0) - G(x)) = 2 \int_{1/L}^{1/a} \frac{1 - \cos(kx) dk}{k^2 + \Sigma(k)} \frac{dk}{2\pi}. \tag{C2}$$

In order to extract the long-distance behavior of this integral, the approximation

$$(1 - \cos(z)) \approx \begin{cases} z^2 & \text{if } z \ll 1 \\ \text{const.} & \text{if } z \gg 1 \end{cases} \tag{C3}$$

is used[93].

In higher dimensions, $d > 1$,

$$(G(\mathbf{0}) - G(\mathbf{r})) = \frac{1}{(2\pi)^d} \int_a^L dk \int d\Omega \frac{1 - e^{i\mathbf{k}\cdot\mathbf{r} \cos \theta}}{k^2 + \Sigma(k)} k^{d-1}. \tag{C4}$$

From Appendix D,

$$\int_0^\pi e^{iz \cos \theta} \sin^{d-2} \theta d\Omega = J_{\frac{d-2}{2}}(z) \left(\frac{z}{2}\right)^{\frac{2-d}{2}} \pi^{1/2} \Gamma\left(\frac{d-1}{2}\right) S_{d-1}. \tag{C5}$$

The asymptotic behavior of $J_\nu(z)$ is

$$J_\nu(z) \approx \begin{cases} \frac{1}{\Gamma(\nu+1)} \left(\frac{z}{2}\right)^\nu \left(1 - \frac{\Gamma(\nu+1)}{2\Gamma(\nu+2)} \left(\frac{z}{2}\right)^2 + \dots\right) & \text{if } z \ll 1 \\ \sqrt{\frac{2}{\pi z}} \cos\left(z - \frac{\pi}{4} - \frac{\nu\pi}{2}\right) & \text{if } z \gg 1 \end{cases} \quad (\text{C6})$$

and

$$\int_0^\pi \sin^{d-2} \theta d\theta = \pi^{1/2} \frac{\Gamma\left(\frac{d-1}{2}\right)}{\Gamma\left(\frac{d}{2}\right)} \quad (\text{C7})$$

Therefore,

$$\int_0^\pi (1 - e^{iz \cos \theta}) \sin^{d-2} \theta d\theta \approx \begin{cases} z^2 \sqrt{\pi} \frac{\Gamma\left(\frac{d-1}{2}\right)}{4\Gamma\left(\frac{d+2}{2}\right)} + \dots & \text{if } z \ll 1 \\ \sqrt{\pi} \frac{\Gamma\left(\frac{d-1}{2}\right)}{\Gamma\left(\frac{d}{2}\right)} & \text{if } z \gg 1 \end{cases} \quad (\text{C8})$$

Since, in the present work, we are only interested in the scaling properties of the quantities investigated, it is sufficient to conclude that after performing the solid angle integrations

(ii) $\Sigma(k) = sk^{\alpha-d}$ where $d < \alpha < d+2$ [94], $k_\times = s^{\frac{1}{2+d-\alpha}}$ and

$$\int (e^{ikr \cos \theta} - 1) d\Omega \propto \begin{cases} (kr)^2 & \text{if } kr \ll 1 \\ \text{const.} & \text{if } 1 \ll kr. \end{cases} \quad (\text{C9})$$

Next, using the above approximations, let us calculate the scaling of $(G(\mathbf{0}) - G(\mathbf{r}))$ when \mathbf{r} is large, for specific forms of $\Sigma(k)$, appearing in the calculations. The crossover wavenumber k_\times is defined by $k_\times^2 = \Sigma(k_\times)$.

(i) $\Sigma(k) = s$, $k_\times = \sqrt{s}$ and

$$\begin{aligned} (G(\mathbf{0}) - G(\mathbf{r})) &\propto r^2 \int_{1/L}^{1/r} \frac{k^2}{s} k^{d-1} dk \\ &+ \int_{1/r}^{k_\times} \frac{k^{d-1} dk}{s} + \int_{k_\times}^{1/a} \frac{k^{d-1} dk}{k^2} \\ &= \begin{cases} s^{-1/2} & \text{if } d = 1 \\ \ln(sa^2) & \text{if } d = 2 \\ a^{2-d} & \text{if } d \geq 3. \end{cases} \quad (\text{C10}) \end{aligned}$$

$$\begin{aligned} (G(\mathbf{0}) - G(\mathbf{r})) &\propto r^2 \int_{1/L}^{1/r} \frac{k^2}{sk^{\alpha-d}} k^{d-1} dk \\ &+ \int_{1/r}^{k_\times} \frac{k^{d-1} dk}{sk^{\alpha-d}} + \int_{k_\times}^{1/a} \frac{k^{d-1} dk}{k^2} \\ &= r^2 \frac{1}{s} [k^{2+2d-\alpha}]_{1/L}^{1/r} + \frac{1}{s} [k^{2d-\alpha}]_{1/r}^{k_\times} \\ &+ [k^{d-2}]_{k_\times}^{1/a} \\ &= \begin{cases} s^{\frac{-1}{3-\alpha}} & \text{if } d = 1 \text{ and } \alpha < 2 \\ \frac{1}{s} \ln(rs) & \text{if } d = 1 \text{ and } \alpha = 2 \\ \frac{1}{s} r^{\alpha-2} & \text{if } d = 1 \text{ and } 2 < \alpha \\ \ln(sa^{\alpha-4}) & \text{if } d = 2 \\ a^{2-d} & \text{if } d \geq 3. \end{cases} \quad (\text{C11}) \end{aligned}$$

(iii) $\Sigma(k) = sk^2 |\ln(ka)|$, $k_\times = \frac{1}{a} e^{1/s}$ and

$$\begin{aligned}
(G(\mathbf{0}) - G(\mathbf{r})) &\propto r^2 \int_{1/L}^{1/r} \frac{k^2}{sk^2 |\ln(ka)|} k^{d-1} dk \\
&+ \int_{1/r}^{k_\times} \frac{k^{d-1} dk}{sk^2 |\ln(ka)|} + \int_{k_\times}^{1/a} \frac{k^{d-1} dk}{k^2} \\
&\propto r^2 \frac{1}{s} [k^{d-2} |\ln(ka)|^{-1}]_{1/L}^{1/r} \\
&+ \frac{1}{s} [(d-2)^{-1} k^{d-2} |\ln(ka)|^{-1}]_{1/r}^{k_\times} \\
&+ [k^{d-2}]_{k_\times}^{1/a} \\
&\propto \begin{cases} \frac{1}{s} \frac{1}{r \ln(r/a)} & \text{if } d = 1 \\ \frac{1}{s} \ln(s \ln(r/a)) & \text{if } d = 2 \\ a^{2-d} & \text{if } d \geq 3. \end{cases} \quad (\text{C12})
\end{aligned}$$

(iv) $\Sigma(k) = sk^2 \ln^{(1-\mu)}(ka)$ in two dimensions while $0 < \mu < 1$. $k_\times = \frac{1}{a} e^{s^{1/(\mu-1)}}$ and

$$\begin{aligned}
G(\mathbf{0}) - G(\mathbf{r}) &= \int_{1/L}^{1/a} \frac{2\pi(1 - J_0(kr))}{k^2 + sk^2 \ln^{1-\mu}(ka)} \frac{k dk}{(2\pi)^2} \\
&\propto \frac{1}{s} \int_{1/r}^{k_\times} \frac{dk}{k \ln^{1-\mu}(ka)} + \dots \\
&\propto \frac{c_2(\mu)}{s} \ln^\mu(r/a) + \mathcal{O}(\ln^{\mu-1}(r/a)), \quad (\text{C13})
\end{aligned}$$

where $c_2(\mu)$ is a constant, the result of the inverse-Fourier transformation.

(v) $\Sigma(k) = sk^2$, $\Sigma(k)$ is negligible to the k^2 term in the integral and the calculation is straightforward

$$(G(\mathbf{0}) - G(\mathbf{r})) \propto \begin{cases} r & \text{if } d = 1 \\ \ln(r/a) & \text{if } d = 2 \\ a^{2-d} & \text{if } d \geq 3. \end{cases} \quad (\text{C14})$$

APPENDIX D: $G(r)$ FOR MASSIVE MODELS

In the literature massive GF are usually appear in their k -space representation:

$$G(k) = \frac{1}{k^2 + m^2}. \quad (\text{D1})$$

In such models the correlation length, in terms of the mass, is

$$\xi = m^{-1}. \quad (\text{D2})$$

Here, the real space behavior of massive GF-s is reviewed.

In one dimension,

$$G(x) = \int_{-\infty}^{\infty} \frac{dk}{2\pi} \frac{e^{ikx}}{k^2 + m^2} = \frac{1}{2m} e^{-mx}, \quad (\text{D3})$$

assuming $x \geq 0$ without loss of generality. The integration was performed using contour integration by completing the integral contour with a semi-circle in the upper half complex plane and using the residuum-theorem with a pole at $k_0 = im$.

In higher dimensions, $d > 1$,

$$G(\mathbf{r}) = \int \frac{d^d k}{(2\pi)^d} \frac{e^{i\mathbf{k}\mathbf{r}}}{k^2 + m^2} \quad (\text{D4})$$

$$= \int \frac{dk k^{d-1}}{(2\pi)^d} \frac{1}{k^2 + m^2} \int d\Omega e^{ikr \cos \theta}. \quad (\text{D5})$$

The integration over the solid angles, $d\Omega$, can be performed

$$\int d\Omega e^{ikr \cos \theta} = S_{d-1} \int_0^\pi d\theta \sin^{d-2} \theta e^{ikr \cos \theta}, \quad (\text{D6})$$

where

$$S_d = \int d\Omega = \frac{2\pi^{d/2}}{\Gamma(d/2)}, \quad (\text{D7})$$

the surface of a d -dimensional unit sphere. From one of the integral representations of the Bessel functions [80],

$$J_\nu(z) = \frac{\left(\frac{z}{2}\right)^\nu}{\pi^{1/2} \Gamma(\nu + 1/2)} \int_0^\pi d\theta \sin^{2\nu} \theta e^{iz \cos \theta} \quad (\text{D8})$$

and

$$\int_0^\infty \frac{t^{\nu+1}}{(t^2 + m^2)^{\mu+1}} J_\nu(at) dt = \frac{a^\mu m^{\nu-\mu}}{2^\mu \Gamma(\mu-1)} K_{\nu-\mu}(am). \quad (\text{D9})$$

As a result,

$$\begin{aligned}
G(r) &= \int \frac{k^{d-1} dk}{(2\pi)^d} \frac{S_{d-1}}{k^2 + m^2} J_{\frac{d-2}{2}}(kr) \frac{\pi^{1/2} \Gamma\left(\frac{d-2}{2} + \frac{1}{2}\right)}{\left(\frac{kr}{2}\right)^{\frac{d-2}{2}}} \\
&= \frac{S_{d-1} \pi^{1/2} \Gamma\left(\frac{d-1}{2}\right) 2^{\frac{d-2}{2}}}{(2\pi)^d} x^{\frac{2-d}{2}} \\
&\times \int_0^\infty dk \frac{k^{d/2}}{k^2 + m^2} J_{\frac{d}{2}-1}(kr) \\
&= \frac{S_{d-1} \pi^{1/2} \Gamma\left(\frac{d-1}{2}\right) 2^{\frac{d-2}{2}}}{(2\pi)^d} r^{\frac{2-d}{2}} m^{\frac{d}{2}-1} K_{\frac{d}{2}-1}(mr) \\
&= (2\pi)^{-d/2} \frac{m^{\frac{d-2}{2}}}{r^{\frac{d-2}{2}}} K_{\frac{d-2}{2}}(mr). \quad (\text{D10})
\end{aligned}$$

The asymptotic behavior of $K_\nu(x)$ is:

If $\nu = 0$,

$$K_0(u) \approx \begin{cases} -\gamma - \ln\left(\frac{u}{2}\right) + \dots & \text{if } u \ll 1 \\ \sqrt{\frac{\pi}{2u}} e^{-u} \left(1 + \mathcal{O}\left(\frac{1}{u}\right)\right) & \text{if } u \gg 1. \end{cases} \quad (\text{D11})$$

If $\nu \neq 0$,

$$K_\nu(u) \approx \begin{cases} \frac{\Gamma(|\nu|)}{2} \left(\frac{2}{u}\right)^{|\nu|} & \text{if } u \ll 1 \\ \sqrt{\frac{\pi}{2u}} e^{-u} \left(1 + \mathcal{O}\left(\frac{1}{u}\right)\right) & \text{if } u \gg 1. \end{cases} \quad (\text{D12})$$

In some examples of the main text, the real space behavior of the one-dimensional massless propagator is needed to know. In Fourier space, $G^0(k) = k^{-2}$. The real space behavior of it can be obtained by

$$\begin{aligned} G(x) &= \frac{1}{2\pi} \int_{2\pi/L}^{2\pi/a} \frac{e^{ikx} dk}{k^2} \approx \frac{1}{2\pi} \int_{2\pi/L}^{\infty} \frac{e^{ikx} dk}{k^2} \\ &= \frac{1}{2\pi} \int_{2\pi/L}^{\infty} \frac{(e^{ikx} - 1) dk}{k^2} + \frac{1}{2\pi} \int_{2\pi/L}^{\infty} \frac{dk}{k^2}. \end{aligned} \quad (\text{D13})$$

First, since our interest is in the case $a \ll r \ll L$ and the integral is convergent at the upper bound so $a \rightarrow 0$ can be taken. Second, a counter term is introduced to the

integrand so as to make the integral convergent at the lower bound too. Next, the $L \rightarrow \infty$ limit can be taken

$$\begin{aligned} G(x) &\approx \frac{1}{2\pi} \int_0^{\infty} \frac{(e^{ikx} - 1) dk}{k^2} + L \\ &= \frac{1}{2\pi} x \int_0^{\infty} \frac{(e^{i\kappa} - 1) d\kappa}{\kappa^2} + L. \end{aligned} \quad (\text{D14})$$

In conclusion

$$G(x) \approx L - x\gamma, \quad (\text{D15})$$

where $\gamma = \frac{1}{2\pi} \int_0^{\infty} \frac{(1 - e^{i\kappa}) d\kappa}{\kappa^2}$ is a constant.

-
- [1] B. Kozma, M.B. Hastings, and G. Korniss, *Phys. Rev. Lett.* **92**, 108701 [4 pages] (2004)
- [2] B. Kozma, M.B. Hastings, and G. Korniss, *Phys. Rev. Lett.* **95**, 018701 [4 pages] (2005).
- [3] R. Albert and A.-L. Barabási, *Rev. Mod. Phys.* **74**, pp. 47–97 (2002).
- [4] S.N. Dorogovtsev and J.F.F. Mendes, *Adv. Phys.* **51**, pp. 1079–1187 (2002).
- [5] M.E.J. Newman, *SIAM Review* **45**, pp. 167–256 (2002).
- [6] S. Boccaletti, V. Latora, Y. Moreno, M. Chavez, and D.-U. Hwang, *Phys. Rep.* **424**, 175–308 (2006).
- [7] D.J. Watts and S.H. Strogatz, *Nature* **393**, pp. 440–442 (1998).
- [8] M.E.J. Newman, *J. Stat. Phys.* **101**, pp. 819–841 (2000).
- [9] S. Milgram, *Psychology Today* **1**, pp. 61–68 (1967).
- [10] P. Erdős and A. Rényi, *Publ. Math. Inst. Hung. Acad. Sci.* **5**, pp. 17–61 (1960).
- [11] B. Bollobás, *Random Graphs* (Cambridge University Press, Cambridge, 2001)
- [12] M.E.J. Newman and D.J. Watts, *Phys. Lett. A* **263**, pp. 341–346 (1999).
- [13] R.T. Scalettar, *Physica A* **170**, pp. 282–290 (1991).
- [14] M. Gitterman, *J. Phys. A* **33**, pp. 8373–8381 (2000).
- [15] A. Barrat and M. Weigt, *Eur. Phys. J. B* **13**, pp. 547–560 (2000).
- [16] M.A. Novotny and S.M. Wheeler, *Braz. J. Phys.* **34**, pp. 395–400 (2004).
- [17] A. Chatterjee and P. Sen, *Phys. Rev E* **74** 036109 (2006)
- [18] B.J. Kim, H. Hong, P. Holme, G.S. Jeon, P. Minnhagen, and M.Y. Choi, *Phys. Rev. E* **64**, 056135 (2001).
- [19] R. Monasson, *Eur. Phys. J. B* **12**, pp. 555–567 (1999).
- [20] S. Jespersen, I.M. Sokolov, and A. Blumen, *Phys. Rev. E* **62**, pp. 4405–4408 (2002).
- [21] S. Jespersen and A. Blumen, *Phys. Rev. E* **62**, pp. 6270–6274 (2002).
- [22] E. Almaas, R.V. Kulkarni, and D. Stroud, *Phys. Rev. Lett.* **88**, 098101 (2002).
- [23] M.B. Hastings, *Eur. Phys. J. B* **42**, pp. 297–301 (2004).
- [24] P.E. Parris and V.M. Kenkre, *Phys. Rev. E* **72**, 056119 (2005).
- [25] F. Jasch and A. Blumen, *Phys. Rev. E* **63**, 041108 (2001).
- [26] J. Lahtinen, J. Kertesz, and K. Kaski, *Phys. Rev. E* **64**, 057105 (2001).
- [27] J. Lahtinen, J. Kertesz, and K. Kaski, *Physica A* **311**, 571 (2002).
- [28] G. Korniss, M.A. Novotny, A.K. Kolakowska, and H. Guclu, SAC 2002, *Proceedings of the 2002 ACM Symposium on Applied Computing*, pp. 132–138 (2002).
- [29] A. Kolakowska, M.A. Novotny, and G. Korniss, *Phys. Rev. E* **67**, 046703 (2003).
- [30] Z. Toroczkai, G. Korniss, M. A. Novotny, and H. Guclu, “Scalability, Random Surfaces, and Synchronized Computing Networks”, in *Computational Complexity and Statistical Physics*, edited by A. Percus, G. Istrate, and C. Moore, Santa Fe Institute Studies in the Sciences of Complexity Series (Oxford University Press, 2006) pp. 249–270.
- [31] G. Korniss, M.A. Novotny, Z. Toroczkai, and P.A. Rikvold, “Nonequilibrium surface growth and scalability of parallel algorithms for large asynchronous systems”, *Computer Simulation Studies in Condensed Matter Physics XIII*, Springer Proceedings in Physics, Vol. 86, editors D.P. Landau, S.P. Lewis, and H.-B. Schüttler (Springer-Verlag, Berlin, Heidelberg), pp. 183–188 (2001).
- [32] H. Guclu and G. Korniss, *Phys. Rev. E* **69**, 065104(R) (2004).
- [33] H. Guclu and G. Korniss, M.A. Novotny, and Z. Rácz, *Phys. Rev. E* **73**, 066115 (2006).
- [34] J. Kleinberg, *Nature* **406**, p. 845 (2000).
- [35] I. M. Sokolov, J. Mai, and A. Blumen, *Phys. Rev. Lett.* **79** 857 (1997)
- [36] P. Sen, K. Banerjee and T. Biswas, *Phys. Rev. E* **66** 037102 (2002).
- [37] C. F. Moukarzel and M. Argollo de Menezes, *Phys. Rev. E* **65**, 056709 (2002)
- [38] M.B. Hastings, *Phys. Rev. Lett.* **91**, 098701 (2003).
- [39] P. Sen and B. K. Chakrabarti, *J. Phys. A* **34**, 7749 (2001)
- [40] P. G. de Gennes, *Scaling Concepts in Polymer Physics* (Cornell University Press, Ithaca, 1979).
- [41] G. Korniss, M.A. Novotny, H. Guclu, Z. Toroczkai, and P.A. Rikvold, *Science* **299**, 677 (2003).
- [42] T. Petermann and P. De Los Rios, *Phys. Rev. E* **73**, 026114 (2006).
- [43] S.B. Laughlin and T.J. Sejnowski, *Science* **301**, pp. 1870–1874 (2003).

- [44] J.A. Davis, V.K. De, and J.D. Meindl, *IEEE Trans. Elec. Dev.* **45**, pp. 580–589 (1998).
- [45] S. E. Halford and J. F. Marko *Nucleic Acid Research* **32**, pp. 3040-3052 (2004).
- [46] Berg and Clas Blomberg, *Biophysical Chemistry* **4**, pp. 367-381 (1976)
- [47] D. Brockmann and T. Geisel, *Phys. Rev. Lett.* **91**, 048303 (2003).
- [48] S. Redner, *A Guide to First-Passage Processes* (Cambridge University Press, Cambridge, UK, 2001).
- [49] S. F. Edwards, D. R. Wilkinson, *Proc. R. Soc. London Ser. A* **381**, 17 (1982)
- [50] A. Nagurney, J. Cruz, J. Dong, and D. Zhang, *European Journal of Operational Research* **26**, 120 (2005).
- [51] B.D. Lubachevsky, *Bell Labs Tech. J.* **5** (April-June), pp. 134–156 (2000).
- [52] A.G. Greenberg, B.D. Lubachevsky, D.M. Nicol, and P.E. Wright, “Efficient Massively parallel simulation of dynamic channel assignment schemes for wireless cellular communications”, *Proc. 8th Workshop on Parallel and Distributed Simulation (PADS’94)*, pp. 187–194 (SCS, San Diego, CA, 1994).
- [53] B.D. Lubachevsky, *Complex Systems* **1**, pp. 1099–1123 (1987).
- [54] B.D. Lubachevsky, *J. Comput. Phys.* **75**, pp. 103–122 (1988).
- [55] R.M. Fujimoto, *Commun. of the ACM* **33**, 30 (1990).
- [56] A.K. Kolakowska and M.A. Novotny, in *Artificial Intelligence and Computer Science*, edited by Susan Shannon, series in *Progress in Computer Science Research* (Nova Science Publishers, Hauppauge, NY, 2005), pp. 151–176.
- [57] G. Korniss, Z. Toroczkai, M.A. Novotny, and P.A. Rikvold, *Phys. Rev. Lett.* **84**, pp. 1351–1354 (2000).
- [58] M. Kardar, G. Parisi, Y.-C. Zhang, *Phys. Rev. Lett.* **56**, 889 (1986)
- [59] A.-L. Barabasi, H. E. Stanley, *Fractal Concepts in Surface Growth*, (Cambridge University Press, 1995)
- [60] F. Y. Wu, *J. Phys. A: Math. Gen.* **37** 6653-6673 (2004)
- [61] E. López, S.V. Buldyrev, S. Havlin, and H.E. Stanley, *Phys. Rev. Lett.* **94**, 248701 (2005).
- [62] Z. Wu, E. López, S.V. Buldyrev, L.A. Braunstein, S. Havlin, and H.E. Stanley, *Phys. Rev. E* **71**, 045101(R) (2005).
- [63] J.S. Andrade, Jr., H.J. Herrmann, R.F.S. Andrade, and L.R. da Silva, *Phys. Rev. Lett.* **94**, 018702 (2005).
- [64] G. Korniss, M.B. Hastings, K.E. Bassler, M.J. Berryman, B. Kozma, D. Abbott, *Physics Letters A* **350**, 324–330 (2006).
- [65] W. J. Tzeng and F. Y. Wu, arXiv:math-ph/0601048
- [66] G. Korniss, *Phys. Rev. E* **75**, 051121 (2007)
- [67] P.G. Doyle and J.L. Snell, *Random Walks and Electric Networks*, Carus Mathematical Monograph Series Vol. 22 (The Mathematical Association of America, Washington, DC, 1984), pp. 83–149; arXiv:math.PR/0001057.
- [68] L. Lovász, *Random Walks on Graphs: A Survey in Combinatorics*, Paul Erdős is Eighty Vol. 2, edited by D. Miklós, V.T. Sós, and T. Szőnyi (János Bolyai Mathematical Society, Budapest, 1996), pp. 353-398;
- [69] A.K. Chandra, P. Raghavan, W.L. Ruzzo, and R. Smolensky, in *Proceedings of the 21st Annual ACM Symposium on the Theory of Computing* (ACM Press, New York, 1989), pp.574–586.
- [70] P. Tetali, *J. Theor. Prob.* **4** 101 (1991).
- [71] L. C. Freeman, *Sociometry* **40**, 35-41 (1977)
- [72] M.E.J. Newman and M. Girvan, *Phys. Rev. E* **69**, 026113 (2004).
- [73] M.E.J. Newman, *Social Networks* **27**, 39–54 (2005).
- [74] R. Guimerà, A. Díaz-Guilera, F. Vega-Redondo, A. Cabrales, and A. Arenas, *Phys. Rev. Lett.* **89**, 248701 (2004).
- [75] B. Danila, Y. Yu, S. Earl, J.A. Marsh, Z. Toroczkai, and K.E. Bassler, *Phys. Rev. E* **74**, 046114 (2006).
- [76] L. Harnau, R. G. Winkler, P. Reineker, *J. Chem. Phys.* **104**, 6355 (1996)
- [77] J. Rammer, *Rev. Mod. Phys.* **63** 781-817 (1991)
- [78] N. Goldenfeld, *Lectures on Phase Transitions and the Renormalization Group*, (Addison-Wesley Publishing Group, 1992)
- [79] W. H. Press et al., *Numerical Recipes in C* (Cambridge University Press, Cambridge, 1995), 2nd ed., Secs. 11.2 and 11.3
- [80] I. S. Gradshteyn, I. M. Ryzhik, *Table of Integrals, Series, and Products*, (Academic Press, 2000)
- [81] One can consider this Hamiltonian as the energy of a given configuration of the surface and the PDF as a finite temperature distribution function of the possible surfaces, in analogy with the PDF of a canonical ensemble in statistical physics.
- [82] In the literature, this construction is also referred to as the pseudo-inverse of the network Laplacian.
- [83] To obtain the above result, one exploits that the GF is defined in the space orthogonal to the zero mode Ψ^0 , hence, $\sum_j G_{ij} = \sum_j \sum_{k=1}^{N-1} \frac{1}{\lambda_k} \Psi_i^k \Psi_j^k = \sqrt{N} \sum_j \sum_{k=1}^{N-1} \frac{1}{\lambda_k} \Psi_i^k \Psi_j^0 = 0$.
- [84] See Eqs. (1) and (47)
- [85] These are the diagrams where all the crosses are connected together by dashed lines. Diagrams with crosses connected to multiple sets by dashed lines are not single-link diagrams, like those of Fig. 9.
- [86] This procedure can also be considered as an *iteration process* since, if the initial ansatz was incorrect, one can take the result of the SCF as a new ansatz of Σ and apply the same steps over and over again until Σ converges to a function that does not change in the iteration process.
- [87] Note that the other two processes which have three GF-s between two endpoints cancel each other
- [88] Note that the fact that the MF approximation is self-consistent grants only that the universal behavior of the quenched and the annealed system will be the same (e.g. the scaling with respect to p) though other features, like constants in the formulae, can exhibit non-universal behavior.
- [89] This property can be obtained by noting that the two constituents of the Hamiltonian, H^0 and qV , must have the same dimension. Also, we know that $H^0 \sim k^2$ and $qV \sim q/L^d$ in Fourier space. Since k has dimension $(length)^{-1}$, the dimensionality of q is $(length)^{d-2}$.
- [90] This is the same criterion as that obtained in Eq. (140).
- [91] The scenario is drastically different for quenched *strongly heterogeneous* (scale-free) networks, where the largest eigenvalue of the network Laplacian is of the order of the largest degree in the network, which scales with a power of the system size N . Thus, the required Δt becomes progressively smaller for larger system sizes.
- [92] The exponent is expressed in this way because of the formulas appearing in the calculations of the perturbation expansion. Note that $0 < \alpha - d < 2$.

[93] Note that, strictly speaking, the large- z approximation is not really accurate: the function oscillates between 0 and 1 but, since it is multiplied with a slowly varying function in Eqn. (74), the approximation is adequate to calculate scaling properties.

[94] The exponent is expressed in this way because of the formulas appearing in the calculations of the perturbation expansion. Note that $0 < \alpha - d < 2$.